Cross sections for $\pi^- + p \to n + k\pi^0$ ($k = 1$ to 5) and $\pi^- + p \to n + \eta^0$ ($\eta^0 \to 2\gamma$) for incident pion momenta between 1.3 and 3.8 GeV/c

H. R. Crouch, Jr.,* R. Hargraves,† R. E. Lanou, Jr., J. T. Massimo, A. E. Pifer,‡ and A. M. Shapiro
Brown University, Providence, Rhode Island 02912

A. E. Brenner,§ M. Ioffredo,‖ and F. D. Rudnick¶
Harvard University, Cambridge, Massachusetts 02138

G. Calvelli, F. Gasparini, L. Guerriero, G. A. Salandin, A. Tomasin, C. Voci, and F. Waldner
Istituto di Fisica dell'Universita di Padova, Padova, Italy

P. Bastien,** B. Brabson,†† B. T. Feld, Y. Goldschmidt-Clermont,‡‡ V. Kistiakowsky, D. Miller,§§ I. A. Pless, A. Rogers,‖‖ L. Rosenson, F. A. Triantis,¶¶ L. Ventura,*** T. L. Watts,††† and R. K. Yamamoto
Massachusetts Institute of Technology, Cambridge, Massachusetts 02139

Y. Eisenberg and E. E. Ronat
Weizmann Institute of Science, Rehovot, Israel
(Received 28 September 1979)

This paper presents the results of a study of the dominant neutral final states from $\pi^- p$ interactions. The data were obtained in an experiment performed at the Brookhaven National Laboratory Alternating Gradient Synchrotron, using a set of steel-plate optical spark chambers surrounding a liquid-hydrogen target. We present differential and total cross sections for the reactions (1) $\pi^- p \to n + \pi^0$ and (2) $\pi^- p \to n + \eta^0$ ($\eta^0 \to 2\gamma$) and total cross sections for the reactions (3) $\pi^- p \to n + k\pi^0$ ($k = 2$, 3, 4, and 5) and (4) $\pi^- p \to$ all neutrals for eighteen values of beam momentum in the interval 1.3 to 4.0 GeV/c. The angular distributions for (1) and (2) have been analyzed in terms of expansions in Legendre polynomials, the coefficients for which are also given.

I. INTRODUCTION

In this paper we report the results of a study of the dominant neutral final states from $\pi^- p$ interactions at eighteen values of the beam momentum in the interval between 1.3 and 4.0 GeV/c. The data were obtained from an experiment performed at the Brookhaven National Laboratory Alternating Gradient Synchroton (AGS), using a set of steel-plate optical spark chambers surrounding a liquid-hydrogen target.

We present total cross sections, angular distributions, and forward differential cross sections for the reactions

$$\pi^- + p \to n + \pi^0 , \tag{1}$$

$$\pi^- + p \to n + \eta^0 \ (\eta^0 \to 2\gamma) , \tag{2}$$

and total cross sections for

$$\pi^- + p \to n + K\pi^0 , \quad K = 2, 3, 4, 5 \tag{3}$$

$$\pi^- + p \to \text{all neutrals} . \tag{4}$$

We have previously published preliminary results from these data,[1] and this paper presents the final results of our analysis and a complete description of the experiment. To facilitate the comparison of these data with theoretical predictions, we present both cross sections and the coefficients obtained by fitting the angular distributions with Legendre-polynomial series in tabular form, as well as presenting cross sections and angular distributions in graphical form.

Other experiments have reported cross sections and angular distributions for π^0 charge exchange [reaction (1)] at lower energies[2]; there are six experiments that overlap the momentum range of the present experiment,[3-9] plus two at higher momenta.[10] However, this paper presents results for the largest number of beam momenta from a single experiment. Three other studies report the results of fits of Legendre-polynomial series to their π^0 data[3-5] and one presents the coefficients obtained from such analysis of their η^0 charge-exchange data [reaction (2)] at five beam momenta.[4] In Sec. V of this paper we present a brief comparison of our data with these other results.

The details of our experiment are described in Sec. II and those of the scanning and measuring of the spark-chamber film in Sec. III. The analysis of the data is discussed in Sec. IV and our results are presented in Sec. V, together with the comparisons with other experiments. Section VI summarizes our results.

II. EXPERIMENTAL SETUP

A. Beam transport

Figure 1 is a plan view of the beam layout. The entire experiment was conducted within the area enclosed by the AGS ring. The beam used in this experiment was designed, and the parameters for it were optimized by a computer-calculated ray-tracing program, to provide 10^3 π^-'s per pulse spread over a region of 3 cm diameter at the target with a momentum resolution of ±0.5% over the momentum range studied. The momentum was selected by the bending magnet and the beam was single-focused by the quadrupole pair. The two pitching magnets, with pitching angle of 4.5°, were used to raise the beam by 38 in. The momentum bite (±0.4%) was mainly determined by the first lead collimator between the beryllium target and bending magnet.

The central momentum of the beam was determined by two independent procedures. A calibrated Hall probe placed inside the bending magnet gave a voltage which was recorded and maintained constant throughout a given momentum run. After correcting for nonlinearity between Hall-probe voltage readings and magnetic field, a set of absolute momenta were calculated. The second procedure was a direct calculation using the magnet current (shunt voltage) and known values of $B_L = \int \vec{B} \cdot d\vec{l}$ for the bending magnet. The two methods agreed to better than 0.6% for all momenta. The beam momentum values assigned to the interaction were corrected by 7.1 MeV/c to compensate for energy loss of the beam in passing through beam defining counters and the aluminum foils of the spark chambers.

The differential Čerenkov counter shown in Fig. 1 was used for determining the contamination of the beam by electrons and muons, and was not used during the data runs. The contamination of the beam was found to be 5% ±0.5% for all beam momenta.

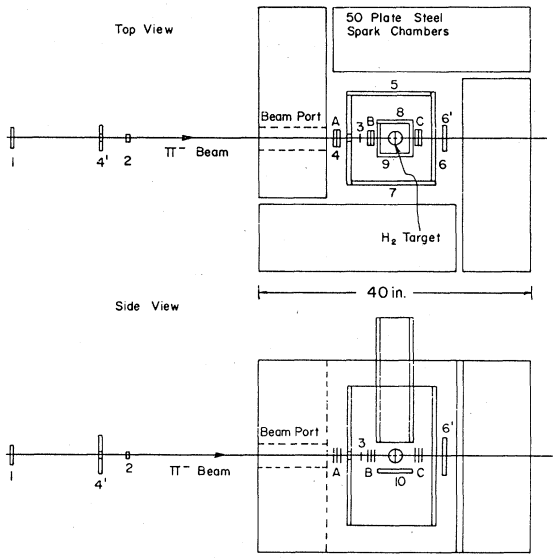

FIG. 2. Schematic showing the scintillation-counter and spark-chamber array.

B. Detector system

Figure 2 shows the detector system which consisted of a scintillation-counter beam telescope and a liquid-hydrogen target surrounded by an array of optical spark chambers and scintillation counters. The hydrogen target was a nearly spherical mylar shell about 4 cm in diameter. It was surrounded by two boxlike arrays of scintillation counters which provided a signal when there were events with charged particles in the final state.

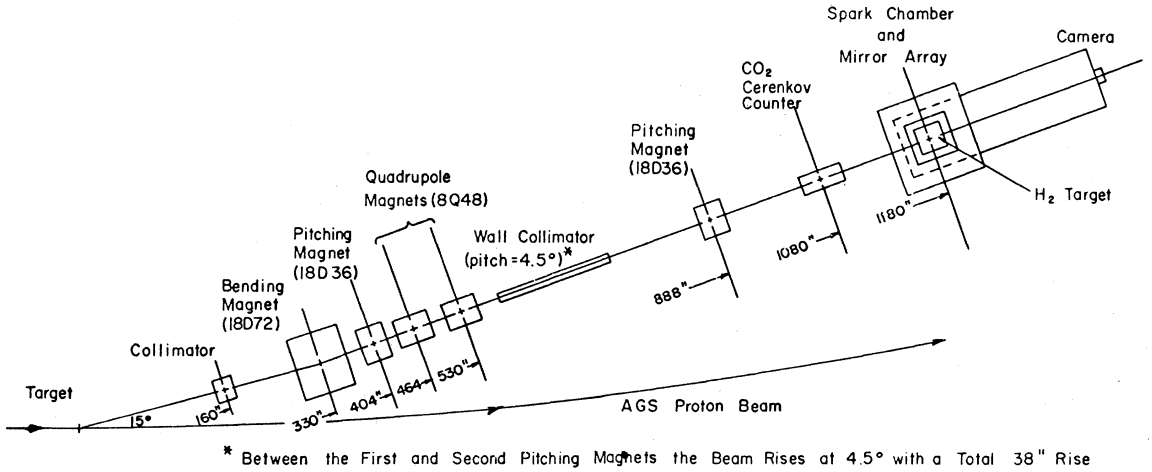

* Between the First and Second Pitching Magnets the Beam Rises at 4.5° with a Total 38" Rise

FIG. 1. Schematic showing the π^- beam line at the AGS and the spark chamber.

Neutral particles, mainly neutrons and photons, usually passed through this anticoincidence array into the steel-plate spark chambers where the photons converted into positron-electron pairs and were detected.

The main spark-chamber array, which is described in detail in Bulos *et al.*,[2] is shown in Fig. 3 together with its system of mirrors. Each of the four chambers was constructed out of fifty 75 cm $\times$75 cm$\times$2 mm-thick steel plates, spaced 3 mm apart, presenting 5.5 radiation lengths of path to photons. Thus, practically all photons convert into positron-electron pairs and about 10% of the neutrons interact in the plates producing visible recoils. A 3.5-in. hole was cut through the 50 plates of the chamber directly facing the incident beam to allow the beam to enter unattenuated and unscattered. Aluminum-foil patches over 15 of the holes allowed beam sparks to be used to locate the incoming track. The boxlike array of the chambers resulted in $\frac{2}{3}$ of the total solid angle being sensitive for photon detection. Each chamber was photographed in two 90° stereo views, and all eight views were recorded by a single 70-mm camera.

The three small, thin-plate spark chambers shown in Fig. 2 and labeled A, B, C were used to further identify the beam. These chambers were constructed of 0.002-in. aluminum foil to minimize interactions with the beam pions and were photographed in 90° stereo by means of their own 45° mirrors.

C. Trigger logic

The incoming beam was defined by requiring signals from scintillation counters 1, 2, and 3 of Fig. 2. Signals from anticoincidence counters 4 and 4′, which have 1-in. holes centered on the beam line, were used to eliminate events where either the beam was off-axis, of the wrong momentum, or possibly interacted in counters 1 or 2 or in the thin foils in the large spark chamber traversed by the beam. Thus a good beam trigger, ensuring that a particle passed through the target, consisted of the five beam counters firing in a $12\bar{3}\bar{4}4'$ configuration. The anticoincidence shield, consisting of counters 4, 5, 6, and 7, detected charged particles leaving the target. In addition, counters 8, 9, and 10 were used to detect charged particles moving only in the nearly vertical direction. Any event of this type was also recorded as such on the film, and approximately 4% of the events with otherwise neutral final states fell into this category.

The small anticoincidence counter 6′ was used to increase the anticoincidence efficiency for noninteracting beam particles. The condition signifying an incoming pion which had produced a neutral final state was thus $12\bar{3}\bar{4}4'5\bar{6}\bar{6}'7$, and the spark chambers were triggered on events satisfying this requirement. Since the triggering of the spark chambers could only take place once per beam spill, neutral events occurring after the first good trigger in a given beam spill could not be recorded. Therefore, in order to obtain the total neutral cross section from the electronic data, the total number of incident pions up to the first good trigger was also recorded for every beam spill.

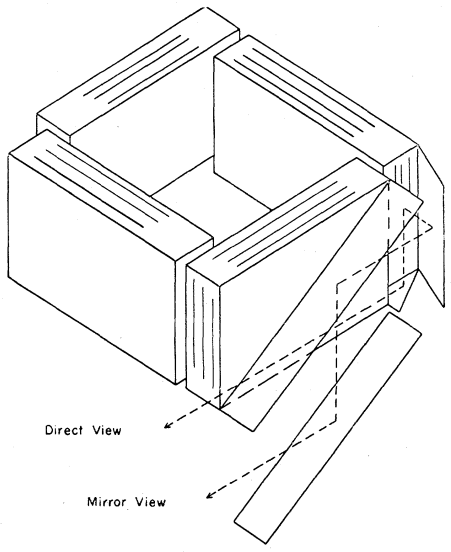

FIG. 3. Schematic showing the arrangement of the spark-chamber sections and the mirrors.

III. FILM SCANNING AND MEASURING

Owing to the relatively high flux of incident particles in the beam, it was necessary to gate the spark-chamber trigger pulse so that it would only be transmitted if there were no previous trigger within ~200 nsec. This allowed ions due to earlier particles to be swept out by the clearing field of the spark chambers. However, particles entering the chamber system during the period (~200 nsec), in which a previous trigger was transmitted and the spark chambers were fired, were also recorded on film, resulting in pictures recording more than one interaction. In order to separate these multiple events from single events, the scanning rules required that the sparks in the entrance region of the spark chamber through which the incoming beam passes be in line with sparks present in small chambers A and B (see Fig. 2). In addition, a good event was further defined by the requirement that there should be no sparks in small chamber C, nor should there be any indication of an interaction of the beam pion before entering the hydrogen target. For total-cross-section analysis,

the multiple events were excluded from the sample, whereas for angular distributions multiple events that were easily separable were used to increase the sample. About 5–40% of the sample consisted of multiple events, depending on the flux of the beam, which varied over a rather wide range.

The films were scanned and measured on image-plane digitizers with setting errors equivalent to $\frac{2}{3}$ mm in space. In each view, four fiducial marks and the first spark of each positron-electron shower were measured. A shower was accepted as such if it had three or more visible sparks (this corresponds to a low-energy cutoff for photons of $\leq$60 MeV energy, as described in Sec. IV A). These measurements were then analyzed by a spatial-reconstruction program which reconstructed the positions of the photon showers with an accuracy of 2.5 mm in space. This overall error, along with the uncertainty of ±1 cm for the interaction point within the hydrogen target, results in an error of $\simeq 2°$ in the overall c.m. system for the opening angle of the photons from π^0 decays.

IV. DATA ANALYSIS

A. Separation of various final states

The observation of events in this experiment depends on the conversion probability of photons in the steel-plate spark chambers. If the conversion probability were unity, and the spark chamber array had 4π sr geometry, the experiment could be performed by essentially counting photons only. However, the conversion probability is not unity, and only $\sim\frac{2}{3}$ of the total solid angle is enclosed by the spark chambers. Therefore, some of the photons are lost, and the main task of the analysis is to correct for these losses.

The losses due to less than 100% geometric acceptance and efficiency of the spark chambers depend in detail on the multiplicity of π^0's in the final state, and the angular and energy distributions of these π^0's. In general, there is no *a priori* knowledge of these angular and energy dependencies, and therefore these functions must be deduced from the data itself. This technique can be successful only if all measured quantities are consistent over the entire energy range. In addition, separate data for the various multiple-π^0 states cannot be obtained and therefore a sufficient amount of data must be available to disentangle the various cross sections and the effects of the detection efficiency on the single π^0 and η^0 samples. For example, due to the limited geometry and photon-conversion probability of the chambers, a $5\pi^0$ final state may appear in the photographs as a ten-photon-shower event or an event containing anywhere from nine to zero photon showers. Hence, various contributions from the $5\pi^0$ final state appear in various photon-shower configurations. An analogous situation is true for the $4\pi^0$, $3\pi^0$, and $2\pi^0$ final states. The procedure used to unscramble the information concerning multiple-π^0 states from the data on the number and disposition of the showers is straightforward, although not *a priori* obvious, and utilizes purely experimental (not theoretical) knowledge. It is based on the following facts and reasonable assumptions:

(1) The two-photon sample is contaminated by partial conversion from four-, six-, eight-, and ten-photon producing parents only. This assumes that there are no significant contributions from sources of odd numbers of photons or more than 10 photons. Although the ω^0 can decay into $\pi^0\gamma$, the relative number of events decaying by this mode is negligible and there is no evidence for other sources that lead to events with an odd number of photons in the final state.

(2) The four-, six-, eight-, and ten-photon producing parents in the final state consist only of 2, 3, 4, and $5\pi^0$ events, respectively. Since there is no evidence for other sources, the exceptions to this statement are assumed to be rare and their effects negligible.

As an example, consider the extraction of $2\pi^0$ parent final states from a sample of four photons. In this four-photon sample, some of the events are due to photon conversions from $2\pi^0$'s, some from partial photon conversions of $3\pi^0$'s where two photons were lost due to detection inefficiencies, while a few may be due to $4\pi^0$'s where four photons were lost. The aim of this analysis is to reconstruct from the directions of the four photons the directions and energies of the two parent neutral pions. The problem involves seven unknowns: the three components of the neutron momentum and the four photon energies. Since there are four energy-momentum constraints and the masses of the pions are known, this results in one more unknown than equations, preventing the solution of this problem on an event-by-event basis. However, there is a statistical approach to the problem which will now be outlined.

A particle isotropically decaying into two photons in its rest frame will display an opening-angle distribution given by

$$\frac{dn}{d\theta} = \frac{\cos\left(\frac{\theta}{2}\right)}{2\sin^2\left(\frac{\theta}{2}\right)\left[\left(\frac{E}{m_0}\right)^2 - 1\right]^{1/2}\left[\left(\frac{E}{m_0}\right)^2 \sin^2\left(\frac{\theta}{2}\right) - 1\right]^{1/2}}, \tag{5}$$

where E is the total energy of the parent particle,

θ the angle subtended by the two photon directions, and m_0 the mass of the parent particle.

Therefore, for a π^0 of energy E, there exists an angle $\theta_{1/2}(E)$ for which half of the π^0's will decay with opening angles smaller than $\theta_{1/2}(E)$, and the remaining half will decay with opening angles larger than $\theta_{1/2}(E)$. In some sense, $\theta_{1/2}(E)$ is the average opening angle from the decay of a π^0 of energy E. Alternatively, on the average, a π^0 that decays with opening angle θ may be considered to have an energy E^* with $\theta = \theta_{1/2}(E^*)$.

This idea can be used to statistically determine the energy and direction for the pions from the known photon direction. To describe the procedure within the framework of our $2\pi^0$ example, the four-photon sample will be taken. There are three different $2\pi^0$ configurations corresponding to the three possible photon pairings. Using the idea of associating with the opening angle a unique π^0 energy (E^*), a total energy can be assigned to each $2\pi^0$ configuration. The $2\pi^0$ configuration having a total energy nearest the beam energy minus 500 MeV is chosen to be the "correct" one. In this way, a sample of π^0's with an assigned energy distribution is produced. For the median opening angle $\theta_{1/2}(E)$ defined above, the actual π^0 direction lies very close to the direction of the opening-angle bisector and, on the average, the bisector represents the π^0 direction. Hence, using the opening-angle bisector for the direction of each π^0, a sample of $2\pi^0$ final state with known pion directions and energies can be defined.

In order to determine the probability that $2\pi^0$ events are detected as four converted photons, the energy and directions of the pions from the "reconstructed" $2\pi^0$ sample are used in conjunction with a Monte Carlo program in the following manner. The geometric configuration of the two π^0's for a given event is held fixed and the π^0's are allowed to decay isotropically in their rest frames. These decay photons are then allowed to traverse through the spark-chamber system and convert randomly into electron-positron pairs according to their energy-dependent conversion lengths. The number of photons that convert in the spark chamber is then recorded. This procedure is repeated nine more times, each time rotating the fixed final-state configuration of π^0's around the incident-beam direction by 36°. Each reconstructed $2\pi^0$ event is in turn treated this way, and thus the probabilities that a $2\pi^0$ event will be observed as an event with zero to four photons can be obtained.

The actual four-photon data sample can be expected to contain events due to three and more pions for which only four photons convert in the spark chambers. This contamination can be greatly reduced by the following technique. Since the probabilities P_{ij} for observing j photons from i π^0's, determined as described in the following paragraphs, indicate that at all energies $\geq 75\%$ of the contamination is due to $3\pi^0$ events, the six-photon sample is used to generate a $3\pi^0$ sample in the manner previously described by which the four-photon sample was used to generate a $2\pi^0$ sample. The $\leq 25\%$ contamination of the six-photon sample by the partial conversions of eight or more protons is ignored at this stage of the process. Next, using Monte Carlo techniques, the $3\pi^0$ final-state configurations obtained from the six-photon events can be systematically rotated and the π^0 "allowed to decay," in order to obtain the fraction of events that appear as four observed photons.

The method described in the above example for reconstructing $2\pi^0$ events was also used for reconstructing $3\pi^0$, $4\pi^0$, and $5\pi^0$ events. These reconstructed events were then "rotated" by Monte Carlo means, as in the case for the $2\pi^0$ example, and the various probabilities P_{ij} for observing j photons from i π^0's ($i = 2, 3, 4, 5$ and $j = 3, 4, 5, \ldots, 10$) were determined. The probability P_{12} was determined using the Monte Carlo program by taking the angle-bisector distribution of the two-photon events for the π^0 distribution. For all energies studied in this experiment, the four-photon sample contained a $\leq 25\%$ contribution from $3\pi^0$ events and a $\leq 8\%$ contribution from $4\pi^0$ and $5\pi^0$ events.

It should be noted here that a minimum energy is required for a photon before it can be unmistakably observed in the spark chambers, and therefore the P_{ij} values depend on this low-energy cutoff. In order to determine the proper energy to use for the cutoff, the Monte Carlo program for determining the P_{ij}'s was run with 50, 60, and 70 MeV photon cutoff energies. The set of P_{ij}'s giving the best agreement between the predicted numbers of events with given photon multiplicity and the experimental observations was considered to correspond to the correct energy cutoff. This value was found to be 60 MeV and has been used throughout the entire analysis.

In order to obtain relatively clean samples of events from which the correlated energy and direction distributions of the parent π^0's could be extracted, the analysis must take into account both the probability that a $2n$ (n = number of parent π^0's) photon event may appear as a $2(n-1)$ photon event by losing both photons from one π^0, and that due to losing one photon from each of the two π^0's. In the first case, the total energy calculated using the pairing technique described above will be less than that for a true $n\pi^0$ event. This almost always holds true for the second case also. Therefore, events with small visible energy were systematically e-

liminated from each $n\pi^0$ event sample, examining the single-photon angular distribution, the two-photon opening-angle distribution, and the three-photon apex cone angle distribution at each step of event elimination. This procedure was continued until the shapes of these distributions stabilized. In all cases, the removal of 10%–20% of the events with least visible energy caused large changes in the three distributions mentioned above. Additional removal of events, however, produced only small gradual changes. This behavior indicates that the events with low visible energies do not really belong to their respective samples and are, in fact, due to misidentification of π^0's from loss of photons. Thus, these events were eliminated and the distributions of $n\pi^0$ parents were determined. Then least-squares fits to the total numbers of three-to-ten-photon events (see Sec. IV D), together with fits to the angular distribution of single photons and the opening-angle distribution of two photons (see Sec. IV B), were carried out to determine the actual number of events for the various $n\pi^0$ parent final states.

As an overall test for the validity of the method used to separate the various final-state events, the sample of observed three-photon events was compared with a sample predicted on the basis of the fitted number of multiple-π^0 parents and the probability for obtaining three photons from these various multiple-π^0 events. The three-photon samples were used for these reliability tests, since no channel resulting in three photons of appreciable cross section is expected in this experiment. Figure 4 gives a comparison of the distributions for the opening angles (three per event) obtained from observed events and Monte Carlo produced events for two typical beam momentum. The predicted samples agree very well with the observed ones, indicating that the method used here to separate the various final states is quite reliable.

B. π^0, η^0 final states

In order to obtain a clean sample of single π^0 and η^0 final-state events, the background due to multiple-π^0 events, in which only two photons convert, was subtracted from the two-photon event sample. The amount of background contribution due to each category of multiple-π^0 events was determined from the fitted number of $n\pi^0$ parents, along with the established probability for observing two photons from n π^0's (P_{n2}, $n=2$, 3, 4, 5). The angular distributions of these background events were obtained from the rotated samples from which only two photon conversions were considered and treated as the decay of a single π^0. The opening-angle

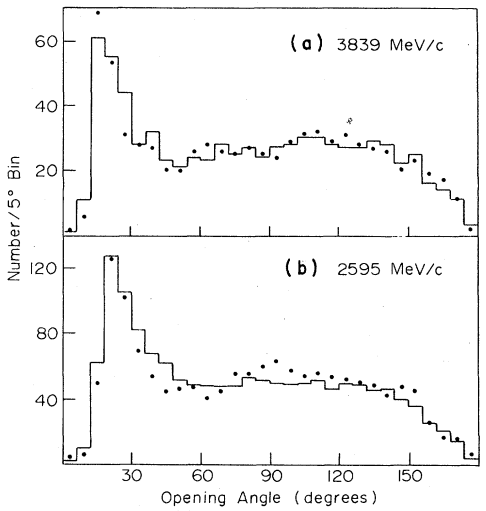

FIG. 4. Opening-angle distributions of the three possible two-photon combinations from three-photon events at two incident pion laboratory momenta. The histogram gives the experimental result and the dots give the Monte Carlo predictions. The χ^2 per number of degrees of freedom was $\chi^2/\mathrm{ND}=\frac{52}{90}$ for (a) and $\frac{57}{90}$ for (b).

distributions obtained for these events are much broader than those from true π^0 decays. Figure 5 gives the opening-angle distribution of two-photon events from π^0 and η^0 final states for two typical beam momenta. The solid curves represent the data including background, while the dashed curves

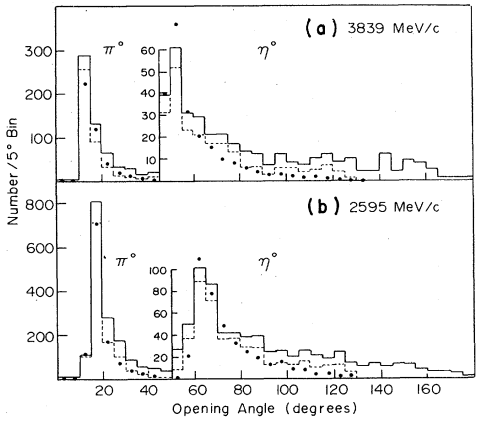

FIG. 5. Opening-angle distributions of two-photon events at two incident pion laboratory momenta. The solid line gives the uncorrected experimental result, the dashed line, the experimental result after background subtraction, and the dots give the Monte Carlo prediction.

represent the data for π^0 and η^0 with the background subtracted. The dots are events predicted by Monte Carlo means, and their good agreement with the dashed curves again indicates the reliability of the analysis.

C. Angular distribution

The angular distributions for charge-exchange π^0 and η^0 production were both determined by the following method. As mentioned in Sec. IV A, a particle of mass m_0 and total energy E, which decays isotropically into two photons within its own rest frame, is characterized by the opening-angle distribution given by Eq. 5. The angle θ_{PB} between the particle's vector momentum and the bisector of the opening angle between the two photons is given by

$$\cos\theta_{PB} = \frac{E\cos\left(\frac{\theta}{2}\right)}{(E^2 - m_0^{\,2})^{1/2}} . \tag{6}$$

The direction of flight of the higher-energy photon will always lie closer to that of the decaying particle, whereas the lower-energy photon will have its direction of flight at a larger angle to that of the particle. Thus, knowledge of the energies of the decay photons, the opening angle between the photons, and the mass and energy of the parent particle allows for a unique determination of the particle's direction of flight. In this experiment, however, the energies of the photons were not determined, and therefore, although the angle between the opening-angle bisector and the parent-particle's direction of flight could be determined, an ambiguity is present concerning on which side of the bisector is the actual direction of flight of the particle. At the minimum opening angle given by

$$\cos\left(\frac{\theta_{\min}}{2}\right) = \frac{(E^2 - m_0^{\,2})^{1/2}}{E} , \tag{7a}$$

or equivalently

$$\sin\left(\frac{\theta_{\min}}{2}\right) = \frac{m_0}{E} , \tag{7b}$$

the ambiguity vanishes and the direction of flight of the parent particle is collinear with the bisector. Since the distribution of opening angles is highly peaked near the minimum opening angle, as can be seen by examination of Eq. 5, most of the events have parent directions nearly collinear with the opening-angle bisector.

In order to extract the angular distribution of the parent particle in the overall $\pi^- p$ c.m. system, the two possible parent-particle directions on either side of the bisector are considered with equal *a priori* probability. The distribution of the cosine of the polar angles for both parent directions ($\cos\theta_p$) is

$$dN(\cos\theta_p) = \int P(\cos\theta_p, \cos\theta_t)\frac{dN(\cos\theta_t)}{d\Omega_t} d\Omega_t , \tag{8}$$

where $dN(\cos\theta_t)/d\Omega_t$ is the true angular distribution of the parent particle, $dN(\cos\theta_p)$ is the observed distribution of the parent particle, and $P(\cos\theta_p, \cos\theta_t)$ is the probability that a parent with true direction $\cos\theta_t$ gives rise to each of the possible $\cos\theta_p$ values.

For fitting purposes, Eq. (8) is rewritten as

$$dN_{pi} = 2\pi\Delta \sum_j \rho_{ij}\frac{dN_{tj}}{d\Omega_t} , \tag{9}$$

where dN_{pi} is the number of events in the ith parent distribution bin, $dN_{tj}/d\Omega_t$ is the number of events per steradian in the jth true parent distribution bin, Δ is the fixed width in $\cos\theta_t$ bins, and ρ_{ij} is the probability array describing the probability that a parent in the jth directional bin appears as a parent in the ith "observed" parent bin. As previously discussed, for every true parent there appear two observed parents due to the ambiguity arising from the lack of knowledge of the photon energies.

The ρ_{ij} array was determined by using Monte Carlo techniques, taking into account the spark-chamber geometry and energy-dependent photon conversion probabilities, and measurement errors. Very briefly, the steps taken in the Monte Carlo algorithm are as follows:

(i) An interaction point is randomly chosen along the beam path within the liquid-H_2 target.

(ii) A parent particle produced together with a neutron is isotropically and randomly chosen in the overall $\pi^- p$ c.m.. The bin corresponding to the index j of ρ_{ij} is then incremented.

(iii) The parent is allowed to decay isotropically in its own rest frame into two photons.

(iv) The energies and directions of the photons are then determined in the overall $\pi^- p$ c.m..

(v) The potential paths of the photons through the spark-chamber system in the laboratory are then established and the photons allowed to convert according to conversion probabilities which take into account the energies of the photons and the various types and amount of material along the photon path.

(vi) When both photons convert within the scan-

TABLE I. Amplitudes and integrated cross sections obtained by fitting the angular distributions for $\pi^- + p \rightarrow n + \pi^0$ with Legendre-polynomial series at 18 incident pion momenta. $A(l)$ is the amplitude for the lth Legendre polynomial, $P(\chi^2)$ gives the confidence level of the fit for each momentum, and σ is the integrated cross section $[\sigma = 4\pi A(0)]$. The numbers in the parentheses are the uncertainties in the amplitudes and cross sections.

P (MeV/c)	$A(0)$	$A(1)$	$A(2)$	$A(3)$	$A(4)$	$A(5)$	$A(6)$	$A(7)$	$A(8)$	$A(9)$	$A(10)$	$A(11)$	$A(12)$	$A(13)$	$A(14)$	$P(\chi^2)$	σ (mb)
1395	0.158	0.001	0.145	0.035	0.027	−0.024	0.027	−0.153	−0.053							0.82	1.99
	(0.008)	(0.008)	(0.012)	(0.013)	(0.015)	(0.017)	(0.020)	(0.024)	(0.026)								(0.10)
1469	0.175	−0.019	0.125	0.090	0.077	−0.059	0.000	−0.106	−0.106							1.00	2.20
	(0.007)	(0.007)	(0.011)	(0.012)	(0.014)	(0.017)	(0.001)	(0.022)	(0.024)								(0.08)
1543	0.144	0.009	0.083	0.120	0.095	−0.001	−0.024	−0.082	−0.042							0.96	1.81
	(0.006)	(0.006)	(0.008)	(0.010)	(0.011)	(0.013)	(0.014)	(0.016)	(0.018)								(0.07)
1697	0.132	0.066	0.087	0.155	0.164	0.074	−0.002	−0.099	−0.011							0.21	1.66
	(0.005)	(0.006)	(0.008)	(0.010)	(0.012)	(0.012)	(0.013)	(0.016)	(0.017)								(0.06)
2025	0.061	0.048	0.064	0.088	0.121	0.070	0.038	0.001	−0.001	0.025	−0.032					0.96	0.77
	(0.003)	(0.004)	(0.006)	(0.007)	(0.009)	(0.009)	(0.010)	(0.011)	(0.011)	(0.013)	(0.014)						(0.04)
2090	0.068	0.050	0.081	0.088	0.126	0.095	0.039	−0.007	0.001	0.042	−0.026					1.00	0.85
	(0.006)	(0.006)	(0.009)	(0.010)	(0.013)	(0.012)	(0.011)	(0.011)	(0.012)	(0.014)	(0.014)						(0.04)
2170	0.058	0.068	0.087	0.078	0.112	0.079	0.040	−0.004	−0.019	0.019	−0.004					0.99	0.73
	(0.003)	(0.005)	(0.007)	(0.007)	(0.009)	(0.010)	(0.011)	(0.012)	(0.013)	(0.014)	(0.014)						(0.04)
2303	0.058	0.057	0.082	0.065	0.097	0.079	0.048	0.008	−0.015	0.013	−0.012					0.84	0.73
	(0.003)	(0.004)	(0.006)	(0.006)	(0.007)	(0.008)	(0.008)	(0.009)	(0.010)	(0.010)	(0.011)						(0.04)
2529	0.046	0.050	0.075	0.059	0.083	0.071	0.063	−0.005	−0.026	−0.041	−0.044	−0.061	−0.003			1.00	0.58
	(0.002)	(0.003)	(0.005)	(0.005)	(0.006)	(0.007)	(0.007)	(0.008)	(0.009)	(0.010)	(0.010)	(0.011)	(0.011)				(0.02)
2595	0.040	0.037	0.063	0.046	0.067	0.059	0.043	−0.008	−0.023	−0.044	−0.038	−0.045	−0.009			0.63	0.50
	(0.002)	(0.003)	(0.004)	(0.005)	(0.006)	(0.006)	(0.007)	(0.007)	(0.008)	(0.009)	(0.009)	(0.010)	(0.010)				(0.02)
2795	0.033	0.048	0.075	0.055	0.067	0.067	0.063	0.010	−0.016	−0.042	−0.048	−0.034	−0.025			0.53	0.41
	(0.002)	(0.003)	(0.005)	(0.005)	(0.006)	(0.006)	(0.006)	(0.006)	(0.007)	(0.008)	(0.009)	(0.009)	(0.010)				(0.02)
3027	0.025	0.037	0.065	0.058	0.065	0.078	0.072	0.038	0.011	−0.005	−0.019	−0.016	−0.007			0.58	0.32
	(0.002)	(0.003)	(0.005)	(0.005)	(0.006)	(0.007)	(0.007)	(0.006)	(0.006)	(0.007)	(0.007)	(0.008)	(0.008)				(0.02)
3101	0.029	0.040	0.071	0.063	0.070	0.082	0.082	0.042	0.006	−0.014	−0.022	−0.028	−0.028			0.63	0.36
	(0.002)	(0.003)	(0.005)	(0.006)	(0.006)	(0.008)	(0.008)	(0.008)	(0.008)	(0.009)	(0.010)	(0.010)	(0.011)				(0.02)
3308	0.023	0.039	0.061	0.050	0.056	0.062	0.062	0.043	0.019	−0.004	−0.011	−0.018	−0.003			0.33	0.29
	(0.001)	(0.002)	(0.003)	(0.004)	(0.004)	(0.005)	(0.005)	(0.005)	(0.005)	(0.006)	(0.006)	(0.006)	(0.006)				(0.01)
3485	0.020	0.036	0.061	0.051	0.061	0.057	0.061	0.045	0.028	0.003	−0.007	−0.014	−0.009			0.56	0.25
	(0.001)	(0.002)	(0.003)	(0.004)	(0.004)	(0.004)	(0.005)	(0.005)	(0.005)	(0.006)	(0.006)	(0.005)	(0.006)				(0.01)
3687	0.017	0.034	0.058	0.052	0.060	0.054	0.059	0.043	0.031	0.007	−0.012	−0.009	−0.024	−0.016	−0.020	0.09	0.21
	(0.001)	(0.002)	(0.003)	(0.004)	(0.004)	(0.004)	(0.005)	(0.005)	(0.005)	(0.005)	(0.005)	(0.006)	(0.006)	(0.006)	(0.007)		(0.01)
3762	0.015	0.025	0.045	0.046	0.048	0.047	0.052	0.038	0.028	0.005	−0.010	−0.012	−0.021	−0.013	−0.020	0.19	0.19
	(0.001)	(0.002)	(0.003)	(0.003)	(0.004)	(0.004)	(0.004)	(0.004)	(0.004)	(0.005)	(0.005)	(0.005)	(0.006)	(0.005)	(0.006)		(0.01)
3839	0.014	0.029	0.052	0.044	0.048	0.060	0.062	0.039	0.023	0.018	0.021	0.002	−0.022			0.11	0.18
	(0.001)	(0.003)	(0.004)	(0.006)	(0.005)	(0.008)	(0.008)	(0.008)	(0.012)	(0.007)	(0.011)	(0.008)	(0.015)				(0.01)

ning fiducial volume of the spark chambers, their coordinates are allowed to randomly vary according to Gaussian distributions with standard deviations σ set to 2.5 mm, corresponding to the actual measurement error distributions.

(vii) The opening angle is then determined from these photon conversion points, including measurement uncertainty, both possible parent directions are evaluated, and the corresponding bins denoted by i of ρ_{ij} are incremented.

(viii) The entire i,j distribution is then divided by the total number of true events created to obtain ρ_{ij}.

The number of j bins (true distribution) was set to 320 for both π^0 and η^0 distributions, and the number of i bins (observed distributions) ranged from 44 to 146 for π^0 distributions and 34 to 46 for η^0 distributions. The variation in the number of observed distribution bins is due to the fact that at least ten events were required in any bin, and adjacent bins were combined in regions of low statistics to satisfy this requirement. The effective widths of the observed distribution bins were therefore not constant.

The angular distributions reported here have been expanded in terms of Legendre polynomials

TABLE II. Amplitudes and integrated cross sections obtained by fitting the angular distributions for $\pi^- + p \to n + \eta^0$ with Legendre-polynomial series at eighteen incident pion momenta. $A(l)$ is the amplitude for the lth Legendre polynomial, $P(\chi^2)$ gives the confidence level of the fit for each momentum, and σ the integrated cross section $[\sigma = 4\pi A(0)]$. The numbers in the parentheses are the uncertainties in the amplitudes and cross sections.

P (MeV/c)	$A(0)$	$A(1)$	$A(2)$	$A(3)$	$A(4)$	$A(5)$	$A(6)$	$P(\chi^2)$	σ (mb)
1395	0.034	0.020	0.009	−0.056	0.005			0.99	0.43
	(0.005)	(0.009)	(0.014)	(0.017)	(0.018)				(0.06)
1469	0.024	0.006	0.008	−0.030	−0.001			0.97	0.30
	(0.003)	(0.005)	(0.008)	(0.010)	(0.011)				(0.04)
1543	0.029	0.008	0.020	−0.030	−0.015			0.96	0.37
	(0.003)	(0.005)	(0.008)	(0.010)	(0.011)				(0.04)
1697	0.025	0.012	0.011	−0.012	−0.001			0.98	0.31
	(0.002)	(0.004)	(0.006)	(0.007)	(0.009)				(0.02)
2025	0.016	0.014	0.034	−0.004	−0.016			0.98	0.20
	(0.003)	(0.006)	(0.010)	(0.012)	(0.013)				(0.02)
2090	0.018	0.002	0.019	−0.012	0.007			0.98	0.22
	(0.003)	(0.003)	(0.005)	(0.005)	(0.006)				(0.04)
2170	0.012	0.011	0.031	−0.008	0.018			1.00	0.15
	(0.002)	(0.005)	(0.008)	(0.008)	(0.010)				(0.02)
2303	0.014	0.007	0.016	0.003	−0.007			0.39	0.17
	(0.001)	(0.002)	(0.003)	(0.004)	(0.004)				(0.01)
2529	0.015	0.010	0.022	0.014	−0.000			0.31	0.19
	(0.001)	(0.002)	(0.003)	(0.004)	(0.004)				(0.01)
2595	0.016	0.004	0.021	0.009	0.003			0.99	0.20
	(0.001)	(0.002)	(0.003)	(0.003)	(0.004)				(0.01)
2795	0.010	0.009	0.021	0.005	0.010			1.00	0.12
	(0.001)	(0.002)	(0.003)	(0.004)	(0.005)				(0.01)
3027	0.010	0.011	0.020	0.005	0.008			0.94	0.13
	(0.001)	(0.002)	(0.003)	(0.003)	(0.003)				(0.01)
3101	0.008	0.002	0.017	−0.002	0.005			0.98	0.10
	(0.001)	(0.002)	(0.003)	(0.003)	(0.004)				(0.01)
3308	0.008	0.007	0.018	0.008	0.009			0.90	0.10
	(0.001)	(0.001)	(0.003)	(0.002)	(0.003)				(0.01)
3485	0.008	0.009	0.019	0.014	0.009	0.009	−0.001	0.99	0.10
	(0.001)	(0.001)	(0.003)	(0.003)	(0.003)	(0.003)	(0.003)		(0.01)
3687	0.007	0.007	0.020	0.009	0.016	0.002	0.001	0.31	0.09
	(0.001)	(0.001)	(0.003)	(0.002)	(0.003)	(0.003)	(0.003)		(0.01)
3762	0.007	0.006	0.018	0.012	0.014	0.004	0.002	0.28	0.09
	(0.001)	(0.001)	(0.002)	(0.002)	(0.003)	(0.002)	(0.002)		(0.01)
3839	0.007	0.007	0.018	0.012	0.007	0.006	−0.001	0.53	0.09
	(0.001)	(0.001)	(0.003)	(0.003)	(0.003)	(0.003)	(0.003)		(0.01)

as follows:

$$\frac{dN(\cos\theta_t)}{d\Omega_t} = \sum_l A_l L_l(\cos\theta_t) \tag{10a}$$

or

$$\frac{dN_{ti}}{d\Omega_t} = \sum_l A_l L_l\,, \tag{10b}$$

where L_l are the Legendre polynomials of order l, and A_l are the amplitudes for the lth moment.

A fit was then carried out by minimizing the following χ^2 function with respect to the A_l:

$$\chi^2 = \sum_i \frac{\left[(dN_{pi})_{\rm obs} - 2\pi\Delta \sum_{j=1}^{320} \sum_{l=0}^{l_{\rm max}} A_l L_{lj} \rho_{ij}\right]}{(dN_{pi})_{\rm obs}}. \tag{11}$$

$l_{\rm max}$ was successively increased until the increase no longer improved the confidence level of the fit. For convenience in the use of these results for phase-shift analyses, the $l_{\rm max}$ chosen was always even.

Table I displays the results of the fits to the angular distribution of the Legendre-polynomial amplitudes for charge exchange and Table II those for η^0 production. The corresponding error matrices for these fits are tabulated in Table III for charge exchange and Table IV for η^0 production. Figures 6 and 7 show the angular distributions calculated from the results of these fits for charge exchange and η^0 production, respectively.

D. Total cross sections

The overall neutral cross section was determined by using the electronic counting rates corrected for an estimated electron and muon fractional contamination of 0.05 ± 0.005. The effective target length was calculated from the spatial distribution of the beam and the geometry of the target. The full-target and empty-target rates were corrected for events with charged-particle final states, as well as for effects of neutron recoils in the veto counter and events in which Dalitz conversion of π^0's simulated events with charged final states. These corrections ranged between 9 and 13%, depending on beam momenta. A 3% correction for neutral hyperon production in which hyperons and strange mesons escaped our detectors before decaying has also been taken into account. Figure 8 displays the overall total cross section as a function of beam momenta.

In order to determine the partial cross sections

TABLE III. Error matrices for the fits of Legendre-polynomial series to the angular distributions for $\pi^- + p \to n + \pi^0$ at eighteen incident pion momenta. The terms in the matrices are $\delta A(i)\delta A(j)$, where $\delta A(i)$ is the uncertainty in the amplitude for the ith Legendre polynomial. The numbers in the parentheses are the exponents for these terms [e.g., 0.601(−4) means 0.601×10^{-4}].

(A) 1395 MeV/c

0.601 (-4)	-0.979 (-5)	0.394 (-4)	0.190 (-4)	0.904 (-6)	-0.493 (-5)	0.526 (-5)	-0.479 (-4)	-0.118 (-4)
	0.643 (-4)	-0.724 (-5)	-0.337 (-5)	0.211 (-4)	-0.131 (-4)	-0.108 (-4)	-0.639 (-6)	-0.110 (-4)
		0.136 (-3)	-0.538 (-5)	0.191 (-5)	0.108 (-4)	-0.878 (-5)	-0.407 (-4)	-0.192 (-4)
			0.160 (-3)	-0.324 (-4)	-0.617 (-5)	0.412 (-4)	-0.348 (-4)	-0.193 (-4)
				0.228 (-3)	-0.300 (-4)	-0.105 (-4)	0.394 (-4)	-0.307 (-4)
					0.305 (-3)	-0.434 (-4)	-0.300 (-5)	0.751 (-4)
						0.407 (-3)	-0.447 (-4)	-0.155 (-4)
							0.555 (-3)	-0.679 (-4)
								0.675 (-3)

TABLE III. (*Continued*)

(B) 1469 MeV/c

0.493 (-4)	-0.104 (-4)	0.196 (-4)	0.278 (-4)	0.138 (-4)	-0.141 (-4)	0.133 (-7)	-0.235 (-4)	-0.187 (-4)
	0.536 (-4)	-0.185 (-5)	-0.449 (-5)	0.149 (-4)	-0.510 (-5)	0.861 (-7)	-0.472 (-5)	-0.790 (-5)
		0.113 (-3)	0.301 (-5)	-0.506 (-5)	0.139 (-4)	0.417 (-7)	-0.318 (-4)	-0.230 (-4)
			0.145 (-3)	-0.786 (-5)	-0.202 (-4)	-0.170 (-6)	-0.144 (-4)	-0.316 (-4)
				0.207 (-3)	-0.214 (-4)	0.891 (-7)	0.386 (-4)	-0.121 (-4)
					0.276 (-3)	0.810 (-7)	-0.162 (-4)	0.661 (-4)
						0.154 (-5)	0.506 (-7)	0.128 (-6)
							0.467 (-3)	-0.142 (-4)
								0.572 (-3)

(C) 1543 MeV/c

0.338 (-4)	-0.270 (-5)	0.119 (-4)	0.264 (-4)	0.148 (-4)	-0.323 (-6)	-0.623 (-5)	-0.143 (-4)	-0.633 (-5)
	0.324 (-4)	0.179 (-5)	-0.142 (-5)	0.144 (-4)	-0.394 (-5)	-0.257 (-5)	-0.425 (-5)	-0.176 (-5)
		0.654 (-4)	0.910 (-5)	0.896 (-6)	0.189 (-4)	-0.514 (-5)	-0.946 (-5)	-0.106 (-4)
			0.998 (-4)	0.745 (-5)	-0.861 (-5)	0.268 (-4)	-0.186 (-4)	-0.758 (-5)
				0.132 (-3)	-0.179 (-5)	-0.171 (-4)	0.326 (-4)	-0.781 (-5)
					0.168 (-3)	0.101 (-5)	-0.140 (-4)	0.500 (-4)
						0.210 (-3)	0.311 (-5)	-0.212 (-4)
							0.272 (-3)	0.146 (-4)
								0.328 (-3)

(D) 1697 MeV/c

0.244 (-4)	0.721 (-5)	0.118 (-4)	0.268 (-4)	0.237 (-4)	0.955 (-5)	-0.246 (-5)	-0.123 (-4)	0.499 (-6)
	0.321 (-4)	0.144 (-4)	0.172 (-4)	0.258 (-4)	0.777 (-5)	-0.274 (-6)	-0.749 (-5)	-0.439 (-5)
		0.613 (-4)	0.237 (-4)	0.186 (-4)	0.290 (-4)	0.998 (-5)	-0.105 (-4)	-0.445 (-5)
			0.970 (-4)	0.386 (-4)	0.240 (-4)	0.308 (-4)	-0.206 (-5)	-0.101 (-6)
				0.136 (-3)	0.314 (-4)	0.149 (-4)	0.327 (-4)	0.174 (-4)
					0.151 (-3)	0.283 (-4)	0.145 (-4)	0.525 (-4)
						0.181 (-3)	0.284 (-4)	0.176 (-4)
							0.241 (-3)	0.395 (-4)
								0.280 (-3)

TABLE III. (*Continued*)

(E) 2025 MeV/c

0.953 (-5)	0.527 (-5)	0.750 (-5)	0.121 (-4)	0.131 (-4)	0.637 (-5)	0.434 (-5)	0.675 (-6)	-0.160 (-5)	0.387 (-5)	-0.399 (-5)
	0.171 (-4)	0.114 (-4)	0.119 (-4)	0.158 (-4)	0.945 (-5)	0.340 (-5)	-0.432 (-6)	0.347 (-5)	-0.213 (-5)	0.411 (-6)
		0.319 (-4)	0.173 (-4)	0.202 (-4)	0.186 (-4)	0.746 (-5)	0.362 (-5)	-0.235 (-5)	0.664 (-5)	-0.544 (-5)
			0.501 (-4)	0.302 (-4)	0.183 (-4)	0.244 (-4)	0.325 (-5)	0.425 (-5)	0.454 (-5)	-0.393 (-5)
				0.728 (-4)	0.353 (-4)	0.169 (-4)	0.245 (-4)	0.769 (-5)	0.363 (-5)	-0.486 (-5)
					0.736 (-4)	0.327 (-4)	0.182 (-4)	0.245 (-4)	0.126 (-4)	0.564 (-6)
						0.939 (-4)	0.286 (-4)	0.212 (-4)	0.365 (-4)	0.358 (-5)
							0.116 (-3)	0.387 (-4)	0.194 (-4)	0.416 (-4)
								0.129 (-3)	0.413 (-4)	0.152 (-4)
									0.159 (-3)	0.403 (-4)
										0.187 (-3)

(F) 2090 MeV/c

0.350 (-4)	0.249 (-4)	0.400 (-4)	0.443 (-4)	0.601 (-4)	0.443 (-4)	0.180 (-4)	-0.282 (-5)	-0.760 (-6)	0.198 (-4)	-0.121 (-4)
	0.327 (-4)	0.363 (-4)	0.382 (-4)	0.512 (-4)	0.366 (-4)	0.150 (-4)	-0.378 (-5)	0.172 (-5)	0.111 (-4)	-0.880 (-5)
		0.734 (-4)	0.613 (-4)	0.810 (-4)	0.643 (-4)	0.253 (-4)	0.144 (-6)	-0.144 (-5)	0.241 (-4)	-0.146 (-4)
			0.943 (-4)	0.937 (-4)	0.703 (-4)	0.410 (-4)	0.284 (-6)	0.453 (-5)	0.259 (-4)	-0.180 (-4)
				0.164 (-3)	0.108 (-3)	0.503 (-4)	0.166 (-4)	0.109 (-4)	0.367 (-4)	-0.193 (-4)
					0.135 (-3)	0.586 (-4)	0.219 (-4)	0.241 (-4)	0.395 (-4)	-0.139 (-4)
						0.110 (-3)	0.362 (-4)	0.324 (-4)	0.421 (-4)	0.621 (-5)
							0.128 (-3)	0.457 (-4)	0.336 (-4)	0.372 (-4)
								0.146 (-3)	0.494 (-4)	0.271 (-4)
									0.184 (-3)	0.449 (-4)
										0.196 (-3)

for the various multiple-π^0 final states ($2\pi^0$, $3\pi^0$, $4\pi^0$, $5\pi^0$), a least-squares fit was carried out by minimizing the quantity

$$\chi^2=\sum_{i,j}\frac{(N_j-P_{ij}n_i)^2}{N_j}, \quad \begin{matrix} i=2,3,4,5 \\ j=2,3,4,\ldots,10 \end{matrix} \tag{12}$$

where

$$N_j^P=\sum_{i=i_{\min}}^{5}P_{ij}n_i, \quad \begin{matrix} i_{\min}\geq\frac{1}{2}j \text{ and } i_{\min}\geq 2 \\ j=2,3,4,5\ldots10 \end{matrix}. \tag{13}$$

Here N_j is the number of observed events with j γ's

TABLE III. (*Continued*)

(G) 2170 MeV/c

0.987 (-5)	0.845 (-5)	0.119 (-4)	0.111 (-4)	0.140 (-4)	0.913 (-5)	0.414 (-5)	0.717 (-6)	-0.325 (-5)	0.210 (-5)	-0.873 (-6)
	0.246 (-4)	0.183 (-4)	0.192 (-4)	0.212 (-4)	0.146 (-4)	0.851 (-5)	-0.187 (-5)	0.569 (-7)	-0.941 (-6)	0.316 (-7)
		0.446 (-4)	0.250 (-4)	0.308 (-4)	0.252 (-4)	0.117 (-4)	0.492 (-5)	-0.466 (-5)	0.604 (-5)	-0.266 (-5)
			0.556 (-4)	0.354 (-4)	0.279 (-4)	0.235 (-4)	0.769 (-5)	0.543 (-5)	0.340 (-5)	0.354 (-5)
				0.819 (-4)	0.427 (-4)	0.309 (-4)	0.228 (-4)	0.858 (-5)	0.116 (-4)	-0.278 (-5)
					0.924 (-4)	0.420 (-4)	0.327 (-4)	0.275 (-4)	0.161 (-4)	0.136 (-4)
						0.112 (-3)	0.446 (-4)	0.353 (-4)	0.395 (-4)	0.134 (-4)
							0.133 (-3)	0.544 (-4)	0.392 (-4)	0.295 (-4)
								0.159 (-3)	0.442 (-4)	0.451 (-4)
									0.190 (-3)	0.437 (-4)
										0.209 (-3)

(H) 2303 MeV/c

0.814 (-5)	0.711 (-5)	0.106 (-4)	0.794 (-5)	0.112 (-4)	0.919 (-5)	0.487 (-5)	0.111 (-5)	-0.288 (-5)	0.208 (-5)	-0.125 (-5)
	0.160 (-4)	0.131 (-4)	0.134 (-4)	0.139 (-4)	0.107 (-4)	0.756 (-5)	-0.109 (-5)	0.742 (-7)	-0.156 (-5)	-0.611 (-6)
		0.308 (-4)	0.189 (-4)	0.234 (-4)	0.177 (-4)	0.890 (-5)	0.620 (-5)	-0.408 (-5)	0.255 (-5)	-0.494 (-5)
			0.349 (-4)	0.246 (-4)	0.202 (-4)	0.157 (-4)	0.470 (-5)	0.458 (-5)	0.788 (-6)	0.358 (-6)
				0.516 (-4)	0.330 (-4)	0.238 (-4)	0.137 (-4)	0.370 (-5)	0.956 (-5)	-0.172 (-5)
					0.591 (-4)	0.317 (-4)	0.225 (-4)	0.130 (-4)	0.100 (-4)	0.480 (-5)
						0.677 (-4)	0.318 (-4)	0.253 (-4)	0.154 (-4)	0.806 (-5)
							0.809 (-4)	0.341 (-4)	0.312 (-4)	0.134 (-4)
								0.980 (-4)	0.352 (-4)	0.276 (-4)
									0.109 (-3)	0.367 (-4)
										0.116 (-3)

and N_j^P its predicted counterpart, n_i is the number of actual events with i π^0's which are to be determined by the fit, and P_{ij} is the probability for observing j γ's from i π^0's as discussed in Sec. IV A. The numbers of charge exchange and η^0 production events were determined from the opening-angle fits after removal of background, as discussed in Sec. IV B, and corrected for losses due to the conversion of only one decay photon or no decay photons by the Monte Carlo techniques previously discuss-

TABLE III. (*Continued*)

(I) 2529 MeV/c

0.433 (-5)	0.369 (-5)	0.642 (-5)	0.476 (-5)	0.607 (-5)	0.509 (-5)	0.470 (-5)	-0.154 (-6)	-0.239 (-5)	-0.204 (-5)	-0.291 (-5)	-0.408 (-5)	-0.291 (-6)
	0.112 (-4)	0.843 (-5)	0.980 (-5)	0.933 (-5)	0.854 (-5)	0.607 (-5)	0.570 (-6)	-0.101 (-5)	-0.473 (-5)	-0.304 (-5)	-0.455 (-5)	-0.820 (-6)
		0.219 (-4)	0.125 (-4)	0.180 (-4)	0.124 (-4)	0.967 (-5)	0.317 (-5)	-0.130 (-5)	-0.397 (-5)	-0.695 (-5)	-0.462 (-5)	-0.128 (-5)
			0.273 (-4)	0.157 (-4)	0.170 (-4)	0.128 (-4)	0.461 (-5)	0.177 (-5)	-0.147 (-5)	-0.252 (-5)	-0.805 (-5)	-0.546 (-6)
				0.376 (-4)	0.205 (-4)	0.216 (-4)	0.899 (-5)	0.358 (-5)	0.141 (-5)	-0.268 (-5)	-0.710 (-5)	-0.501 (-5)
					0.443 (-4)	0.216 (-4)	0.193 (-4)	0.111 (-4)	0.435 (-5)	0.241 (-5)	-0.105 (-5)	0.335 (-6)
						0.540 (-4)	0.212 (-4)	0.224 (-4)	0.118 (-4)	0.655 (-5)	0.386 (-5)	0.559 (-5)
							0.614 (-4)	0.244 (-4)	0.295 (-4)	0.174 (-4)	0.101 (-4)	0.601 (-5)
								0.762 (-4)	0.297 (-4)	0.354 (-4)	0.167 (-4)	0.974 (-5)
									0.932 (-4)	0.307 (-4)	0.397 (-4)	0.179 (-4)
										0.108 (-3)	0.312 (-4)	0.381 (-4)
											0.114 (-3)	0.257 (-4)
												0.130 (-3)

(J) 2595 MeV/c

0.410 (-5)	0.299 (-5)	0.596 (-5)	0.414 (-5)	0.502 (-5)	0.507 (-5)	0.298 (-5)	-0.592 (-7)	-0.216 (-5)	-0.305 (-5)	-0.268 (-5)	-0.390 (-5)	-0.396 (-7)
	0.928 (-5)	0.667 (-5)	0.737 (-5)	0.791 (-5)	0.515 (-5)	0.539 (-5)	-0.106 (-5)	-0.104 (-5)	-0.429 (-5)	-0.455 (-5)	-0.278 (-5)	-0.371 (-5)
		0.187 (-4)	0.106 (-4)	0.138 (-4)	0.118 (-4)	0.524 (-5)	0.274 (-5)	-0.317 (-5)	-0.580 (-5)	-0.465 (-5)	-0.744 (-5)	0.113 (-6)
			0.214 (-4)	0.134 (-4)	0.125 (-4)	0.102 (-4)	0.276 (-6)	0.953 (-6)	-0.316 (-5)	-0.556 (-5)	-0.423 (-5)	-0.446 (-5)
				0.304 (-4)	0.169 (-4)	0.149 (-4)	0.622 (-5)	-0.991 (-8)	-0.222 (-5)	-0.311 (-5)	-0.716 (-5)	-0.273 (-5)
					0.359 (-4)	0.157 (-4)	0.136 (-4)	0.589 (-5)	-0.840 (-6)	0.264 (-6)	-0.393 (-5)	-0.210 (-5)
						0.432 (-4)	0.131 (-4)	0.167 (-4)	0.734 (-5)	-0.265 (-6)	0.338 (-5)	-0.656 (-6)
							0.511 (-4)	0.173 (-4)	0.206 (-4)	0.139 (-4)	0.207 (-5)	0.649 (-5)
								0.612 (-4)	0.230 (-4)	0.236 (-4)	0.147 (-4)	0.235 (-5)
									0.756 (-4)	0.261 (-4)	0.307 (-4)	0.150 (-4)
										0.881 (-4)	0.246 (-4)	0.278 (-4)
											0.956 (-4)	0.211 (-4)
												0.102 (-3)

TABLE III. (*Continued*)

(K) 2795 MeV/c

0.370 (-5)	0.468 (-5)	0.761 (-5)	0.546 (-5)	0.619 (-5)	0.627 (-5)	0.589 (-5)	0.104 (-5)	-0.153 (-5)	-0.374 (-5)	-0.443 (-5)	-0.270 (-5)	-0.246 (-5)
	0.111 (-4)	0.120 (-4)	0.109 (-4)	0.111 (-4)	0.107 (-4)	0.933 (-5)	0.246 (-5)	-0.193 (-5)	-0.613 (-5)	-0.632 (-5)	-0.533 (-5)	-0.253 (-5)
		0.237 (-4)	0.165 (-4)	0.199 (-4)	0.169 (-4)	0.145 (-4)	0.401 (-5)	-0.203 (-5)	-0.785 (-5)	-0.114 (-4)	-0.746 (-5)	-0.748 (-5)
			0.233 (-4)	0.178 (-4)	0.185 (-4)	0.140 (-4)	0.473 (-5)	0.879 (-6)	-0.498 (-5)	-0.644 (-5)	-0.749 (-5)	-0.478 (-5)
				0.313 (-4)	0.217 (-4)	0.215 (-4)	0.897 (-5)	0.118 (-5)	-0.273 (-5)	-0.702 (-5)	-0.489 (-5)	-0.563 (-5)
					0.366 (-4)	0.243 (-4)	0.156 (-4)	0.694 (-5)	-0.225 (-5)	-0.258 (-5)	-0.193 (-5)	-0.255 (-5)
						0.421 (-4)	0.195 (-4)	0.145 (-4)	0.521 (-5)	0.226 (-6)	0.938 (-6)	0.769 (-6)
							0.406 (-4)	0.213 (-4)	0.211 (-4)	0.120 (-4)	0.640 (-5)	0.389 (-5)
								0.524 (-4)	0.273 (-4)	0.277 (-4)	0.136 (-4)	0.976 (-5)
									0.667 (-4)	0.323 (-4)	0.315 (-4)	0.161 (-4)
										0.787 (-4)	0.303 (-4)	0.300 (-4)
											0.747 (-4)	0.227 (-4)
												0.911 (-4)

(L) 3027 MeV/c

0.344 (-5)	0.463 (-5)	0.807 (-5)	0.713 (-5)	0.747 (-5)	0.910 (-5)	0.787 (-5)	0.419 (-5)	0.121 (-5)	-0.566 (-6)	-0.216 (-5)	-0.170 (-5)	-0.786 (-6)
	0.101 (-4)	0.132 (-4)	0.127 (-4)	0.137 (-4)	0.141 (-4)	0.133 (-4)	0.679 (-5)	0.224 (-5)	-0.100 (-5)	-0.314 (-5)	-0.309 (-5)	-0.154 (-5)
		0.253 (-4)	0.218 (-4)	0.236 (-4)	0.261 (-4)	0.220 (-4)	0.133 (-4)	0.413 (-5)	-0.696 (-6)	-0.529 (-5)	-0.486 (-5)	-0.255 (-5)
			0.262 (-4)	0.242 (-4)	0.268 (-4)	0.239 (-4)	0.127 (-4)	0.709 (-5)	0.190 (-6)	-0.376 (-5)	-0.370 (-5)	-0.257 (-5)
				0.338 (-4)	0.319 (-4)	0.294 (-4)	0.190 (-4)	0.778 (-5)	0.401 (-5)	-0.284 (-5)	-0.347 (-5)	-0.178 (-5)
					0.458 (-4)	0.370 (-4)	0.251 (-4)	0.145 (-4)	0.464 (-5)	0.223 (-6)	-0.310 (-5)	-0.122 (-5)
						0.478 (-4)	0.289 (-4)	0.198 (-4)	0.119 (-4)	0.192 (-5)	0.298 (-5)	0.105 (-5)
							0.401 (-4)	0.232 (-4)	0.189 (-4)	0.131 (-4)	0.639 (-5)	0.613 (-5)
								0.411 (-4)	0.246 (-4)	0.212 (-4)	0.135 (-4)	0.388 (-5)
									0.505 (-4)	0.275 (-4)	0.210 (-4)	0.180 (-4)
										0.555 (-4)	0.291 (-4)	0.210 (-4)
											0.574 (-4)	0.170 (-4)
												0.606 (-4)

TABLE III. (*Continued*)

(M) 3101 MeV/*c*

0.396 (-5)	0.473 (-5)	0.847 (-5)	0.771 (-5)	0.782 (-5)	0.870 (-5)	0.862 (-5)	0.504 (-5)	0.506 (-6)	-0.183 (-5)	-0.159 (-5)	-0.269 (-5)	-0.361 (-5)
	0.119 (-4)	0.140 (-4)	0.138 (-4)	0.145 (-4)	0.150 (-4)	0.142 (-4)	0.722 (-5)	0.276 (-5)	-0.743 (-6)	-0.421 (-5)	-0.402 (-5)	-0.223 (-5)
		0.288 (-4)	0.231 (-4)	0.259 (-4)	0.276 (-4)	0.242 (-4)	0.141 (-4)	0.486 (-5)	-0.131 (-5)	-0.541 (-5)	-0.701 (-5)	-0.654 (-5)
			0.327 (-4)	0.272 (-4)	0.285 (-4)	0.277 (-4)	0.174 (-4)	0.566 (-5)	-0.130 (-5)	0.606 (-6)	-0.506 (-5)	-0.108 (-4)
				0.417 (-4)	0.349 (-4)	0.350 (-4)	0.226 (-4)	0.108 (-4)	0.551 (-5)	-0.146 (-5)	-0.239 (-5)	-0.430 (-5)
					0.565 (-4)	0.408 (-4)	0.293 (-4)	0.214 (-4)	0.934 (-5)	0.362 (-6)	-0.355 (-5)	0.237 (-5)
						0.639 (-4)	0.385 (-4)	0.245 (-4)	0.158 (-4)	0.912 (-5)	0.252 (-5)	-0.462 (-5)
							0.602 (-4)	0.293 (-4)	0.235 (-4)	0.237 (-4)	0.128 (-4)	-0.553 (-5)
								0.669 (-4)	0.379 (-4)	0.277 (-4)	0.191 (-4)	0.207 (-4)
									0.822 (-4)	0.303 (-4)	0.298 (-4)	0.382 (-4)
										0.909 (-4)	0.398 (-4)	0.165 (-4)
											0.912 (-4)	0.237 (-4)
												0.130 (-3)

(N) 3308 MeV/*c*

0.124 (-5)	0.181 (-5)	0.291 (-5)	0.241 (-5)	0.244 (-5)	0.270 (-5)	0.247 (-5)	0.179 (-5)	0.743 (-6)	-0.607 (-7)	-0.377 (-6)	-0.646 (-6)	0.596 (-7)
	0.517 (-5)	0.566 (-5)	0.586 (-5)	0.582 (-5)	0.547 (-5)	0.539 (-5)	0.357 (-5)	0.191 (-5)	-0.569 (-7)	-0.858 (-6)	-0.982 (-6)	-0.794 (-6)
		0.107 (-4)	0.899 (-5)	0.999 (-5)	0.946 (-5)	0.804 (-5)	0.644 (-5)	0.336 (-5)	0.688 (-6)	-0.351 (-6)	-0.161 (-5)	-0.432 (-6)
			0.128 (-4)	0.111 (-4)	0.115 (-4)	0.993 (-5)	0.694 (-5)	0.494 (-5)	0.237 (-5)	0.470 (-6)	-0.629 (-6)	-0.383 (-6)
				0.167 (-4)	0.138 (-4)	0.139 (-4)	0.103 (-4)	0.684 (-5)	0.429 (-5)	0.231 (-5)	0.517 (-6)	0.436 (-6)
					0.209 (-4)	0.162 (-4)	0.154 (-4)	0.101 (-4)	0.596 (-5)	0.452 (-5)	0.186 (-5)	0.104 (-5)
						0.252 (-4)	0.173 (-4)	0.157 (-4)	0.997 (-5)	0.604 (-5)	0.381 (-5)	0.288 (-5)
							0.273 (-4)	0.175 (-4)	0.166 (-4)	0.104 (-4)	0.554 (-5)	0.547 (-5)
								0.298 (-4)	0.183 (-4)	0.176 (-4)	0.979 (-5)	0.450 (-5)
									0.343 (-4)	0.205 (-4)	0.179 (-4)	0.100 (-4)
										0.369 (-4)	0.181 (-4)	0.166 (-4)
											0.339 (-4)	0.136 (-4)
												0.359 (-4)

TABLE III. (*Continued*)

(O) 3485 MeV/c

0.115 (-5)	0.185 (-5)	0.319 (-5)	0.249 (-5)	0.286 (-5)	0.263 (-5)	0.261 (-5)	0.195 (-5)	0.105 (-5)	0.181 (-6)	-0.436 (-6)	-0.603 (-6)	-0.421 (-6)
	0.521 (-5)	0.607 (-5)	0.653 (-5)	0.619 (-5)	0.591 (-5)	0.568 (-5)	0.399 (-5)	0.273 (-5)	0.172 (-6)	-0.288 (-6)	-0.119 (-5)	-0.487 (-6)
		0.119 (-4)	0.961 (-5)	0.118 (-4)	0.984 (-5)	0.943 (-5)	0.718 (-5)	0.422 (-5)	0.150 (-5)	-0.903 (-6)	-0.105 (-5)	-0.163 (-5)
			0.131 (-4)	0.118 (-4)	0.124 (-4)	0.104 (-4)	0.776 (-5)	0.578 (-5)	0.205 (-5)	0.146 (-5)	-0.110 (-5)	0.810 (-7)
				0.177 (-4)	0.143 (-4)	0.152 (-4)	0.108 (-4)	0.760 (-5)	0.467 (-5)	0.133 (-5)	0.607 (-6)	-0.896 (-6)
					0.201 (-4)	0.163 (-4)	0.156 (-4)	0.108 (-4)	0.612 (-5)	0.473 (-5)	0.133 (-5)	0.145 (-5)
						0.242 (-4)	0.176 (-4)	0.166 (-4)	0.970 (-5)	0.618 (-5)	0.322 (-5)	0.168 (-5)
							0.255 (-4)	0.177 (-4)	0.166 (-4)	0.966 (-5)	0.533 (-5)	0.347 (-5)
								0.282 (-4)	0.175 (-4)	0.183 (-4)	0.782 (-5)	0.571 (-5)
									0.309 (-4)	0.178 (-4)	0.173 (-4)	0.672 (-5)
										0.348 (-4)	0.151 (-4)	0.181 (-4)
											0.278 (-4)	0.101 (-4)
												0.308 (-4)

(P) 3687 MeV/c

0.101 (-5)	0.184 (-5)	0.316 (-5)	0.270 (-5)	0.306 (-5)	0.273 (-5)	0.291 (-5)	0.207 (-5)	0.139 (-5)	0.417 (-6)	-0.728 (-6)	-0.395 (-6)	-0.125 (-5)	-0.699 (-6)	-0.996 (-6)
	0.490 (-5)	0.654 (-5)	0.683 (-5)	0.680 (-5)	0.639 (-5)	0.640 (-5)	0.471 (-5)	0.327 (-5)	0.490 (-6)	-0.818 (-6)	-0.149 (-5)	-0.209 (-5)	-0.211 (-5)	-0.198 (-5)
		0.122 (-4)	0.108 (-4)	0.126 (-4)	0.106 (-4)	0.111 (-4)	0.820 (-5)	0.540 (-5)	0.187 (-5)	-0.212 (-5)	-0.101 (-5)	-0.458 (-5)	-0.294 (-5)	-0.400 (-5)
			0.132 (-4)	0.126 (-4)	0.126 (-4)	0.116 (-4)	0.858 (-5)	0.665 (-5)	0.228 (-5)	-0.320 (-6)	-0.166 (-5)	-0.290 (-5)	-0.311 (-5)	-0.270 (-5)
				0.173 (-4)	0.144 (-4)	0.152 (-4)	0.112 (-4)	0.826 (-5)	0.462 (-5)	0.553 (-7)	-0.154 (-6)	-0.373 (-5)	-0.153 (-5)	-0.313 (-5)
					0.176 (-4)	0.160 (-4)	0.138 (-4)	0.102 (-4)	0.563 (-5)	0.242 (-5)	0.138 (-5)	-0.138 (-5)	-0.197 (-5)	-0.251 (-5)
						0.218 (-4)	0.164 (-4)	0.142 (-4)	0.779 (-5)	0.412 (-5)	0.387 (-5)	-0.245 (-6)	-0.238 (-5)	-0.430 (-5)
							0.209 (-4)	0.152 (-4)	0.132 (-4)	0.752 (-5)	0.664 (-5)	0.262 (-5)	0.192 (-5)	-0.902 (-6)
								0.228 (-4)	0.155 (-4)	0.143 (-4)	0.805 (-5)	0.652 (-5)	0.532 (-5)	0.382 (-5)
									0.251 (-4)	0.161 (-4)	0.155 (-4)	0.976 (-5)	0.897 (-5)	0.786 (-5)
										0.288 (-4)	0.174 (-4)	0.188 (-4)	0.112 (-4)	0.990 (-5)
											0.314 (-4)	0.180 (-4)	0.155 (-4)	0.350 (-5)
												0.369 (-4)	0.162 (-4)	.198 (-4)
													0.394 (-4)	0.231 (-4)
														0.465 (-4)

TABLE III. (*Continued*)

(Q) 3762 MeV/c

0.970 (-6)	0.154 (-5)	0.270 (-5)	0.261 (-5)	0.259 (-5)	0.253 (-5)	0.268 (-5)	0.187 (-5)	0.134 (-5)	0.268 (-6)	-0.593 (-6)	-0.565 (-6)	-0.113 (-5)	-0.628 (-6)	-0.105 (-5)
	0.376 (-5)	0.503 (-5)	0.549 (-5)	0.533 (-5)	0.499 (-5)	0.497 (-5)	0.376 (-5)	0.245 (-5)	0.416 (-6)	-0.698 (-6)	-0.144 (-5)	-0.170 (-5)	-0.150 (-5)	-0.166 (-5)
		0.941 (-5)	0.910 (-5)	0.982 (-5)	0.886 (-5)	0.888 (-5)	0.654 (-5)	0.463 (-5)	0.120 (-5)	-0.146 (-5)	-0.165 (-5)	-0.353 (-5)	-0.189 (-5)	-0.300 (-5)
			0.117 (-4)	0.108 (-4)	0.111 (-4)	0.104 (-4)	0.754 (-5)	0.568 (-5)	0.186 (-5)	-0.792 (-6)	-0.192 (-5)	-0.294 (-5)	-0.218 (-5)	-0.289 (-5)
				0.141 (-4)	0.123 (-4)	0.130 (-4)	0.968 (-5)	0.675 (-5)	0.312 (-5)	-0.215 (-7)	-0.126 (-5)	-0.277 (-5)	-0.194 (-5)	-0.315 (-5)
					0.157 (-4)	0.142 (-4)	0.123 (-4)	0.909 (-5)	0.426 (-5)	0.143 (-5)	0.553 (-6)	-0.219 (-5)	-0.128 (-5)	-0.265 (-5)
						0.192 (-4)	0.145 (-4)	0.127 (-4)	0.695 (-5)	0.325 (-5)	0.146 (-5)	-0.666 (-6)	-0.151 (-5)	-0.310 (-5)
							0.183 (-4)	0.135 (-4)	0.115 (-4)	0.628 (-5)	0.409 (-5)	0.159 (-5)	0.920 (-6)	-0.153 (-5)
								0.201 (-4)	0.130 (-4)	0.121 (-4)	0.746 (-5)	0.461 (-5)	0.352 (-5)	0.194 (-5)
									0.210 (-4)	0.142 (-4)	0.138 (-4)	0.896 (-5)	0.521 (-5)	0.347 (-5)
										0.244 (-4)	0.160 (-4)	0.171 (-4)	0.770 (-5)	0.577 (-5)
											0.277 (-4)	0.159 (-4)	0.152 (-4)	0.528 (-5)
												0.340 (-4)	0.140 (-4)	0.206 (-4)
													0.276 (-4)	0.109 (-4)
														0.320 (-4)

(R) 3839 MeV/c

0.116 (-5)	0.190 (-5)	0.364 (-5)	0.338 (-5)	0.345 (-5)	0.360 (-5)	0.336 (-5)	0.290 (-5)	0.225 (-5)	0.784 (-6)	0.620 (-6)	0.147 (-6)	-0.367 (-6)
	0.722 (-5)	0.882 (-5)	0.347 (-5)	0.479 (-5)	0.156 (-4)	0.156 (-4)	-0.116 (-5)	-0.820 (-5)	0.790 (-5)	0.120 (-4)	-0.997 (-6)	-0.175 (-4)
		0.159 (-4)	0.898 (-5)	0.117 (-4)	0.219 (-4)	0.211 (-4)	0.469 (-5)	-0.357 (-5)	0.920 (-5)	0.134 (-4)	0.984 (-7)	-0.176 (-4)
			0.307 (-4)	0.261 (-4)	-0.447 (-5)	-0.559 (-5)	0.347 (-4)	0.475 (-4)	-0.985 (-5)	-0.260 (-4)	0.621 (-5)	0.482 (-4)
				0.295 (-4)	0.304 (-5)	0.424 (-5)	0.314 (-4)	0.398 (-4)	-0.214 (-5)	-0.179 (-4)	0.383 (-5)	0.343 (-4)
					0.629 (-4)	0.573 (-4)	-0.148 (-4)	-0.436 (-4)	0.359 (-4)	0.593 (-4)	-0.540 (-5)	-0.783 (-4)
						0.673 (-4)	-0.913 (-5)	-0.380 (-4)	0.375 (-4)	0.629 (-4)	0.865 (-5)	-0.726 (-4)
							0.692 (-4)	0.792 (-4)	-0.790 (-5)	-0.309 (-4)	0.273 (-4)	0.845 (-4)
								0.136 (-3)	-0.224 (-4)	-0.602 (-4)	0.167 (-4)	0.148 (-3)
									0.551 (-4)	0.485 (-4)	0.845 (-5)	-0.510 (-4)
										0.117 (-3)	0.127 (-4)	-0.840 (-4)
											0.664 (-4)	0.291 (-4)
												0.238 (-3)

TABLE IV. Error matrices for the fits of Legendre-polynomial series of Legendre-polynomial series to the angular distributions for $\pi^- + p \rightarrow n + \eta^0$ at eighteen incident pion momenta. The terms in the matrices are $\delta A(i)\delta A(i)$, where $\delta A(i)$ is the uncertainty in the amplitude for the ith Legendre polynomial. The numbers in the parentheses are the exponents for these terms [e.g., 0.265(−4) means 0.265×10^{-4}].

(A) 1395 MeV/c

0.265 (-4)	0.569 (-7)	0.133 (-4)	-0.308 (-4)	0.305 (-5)
	0.753 (-4)	-0.566 (-4)	0.152 (-4)	0.138 (-5)
		0.191 (-3)	-0.918 (-4)	0.388 (-4)
			0.296 (-3)	-0.958 (-4)
				0.322 (-3)

(B) 1469 MeV/c

0.975 (-5)	-0.184 (-5)	0.473 (-5)	-0.863 (-5)	0.724 (-6)
	0.259 (-4)	-0.205 (-4)	0.973 (-5)	0.146 (-5)
		0.721 (-4)	-0.323 (-4)	0.125 (-4)
			0.102 (-3)	-0.309 (-4)
				0.120 (-3)

(C) 1543 MeV/c

0.981 (-5)	-0.104 (-5)	0.480 (-5)	-0.663 (-5)	-0.371 (-5)
	0.228 (-4)	-0.158 (-4)	0.307 (-5)	-0.217 (-7)
		0.644 (-4)	-0.298 (-4)	0.391 (-5)
			0.978 (-4)	-0.332 (-4)
				0.117 (-3)

(D) 1697 MeV/c

0.525 (-5)	0.777 (-7)	0.781 (-6)	-0.329 (-6)	-0.173 (-6)
	0.129 (-4)	-0.385 (-5)	0.123 (-6)	0.332 (-5)
		0.343 (-4)	-0.878 (-5)	0.579 (-6)
			0.542 (-4)	-0.123 (-4)
				0.762 (-4)

(E) 2025 MeV/c

0.925 (-5)	-0.464 (-5)	0.973 (-5)	-0.196 (-7)	-0.346 (-5)
	0.382 (-4)	-0.221 (-4)	0.147 (-4)	0.134 (-5)
		0.108 (-3)	-0.532 (-4)	0.203 (-4)
			0.152 (-3)	-0.624 (-4)
				0.178 (-3)

(F) 2090 MeV/c

0.699 (-5)	-0.393 (-6)	0.677 (-5)	-0.388 (-5)	0.215 (-5)
	0.661 (-5)	-0.288 (-5)	0.164 (-5)	0.173 (-5)
		0.230 (-4)	-0.965 (-5)	0.480 (-5)
			0.277 (-4)	-0.102 (-4)
				0.366 (-4)

(G) 2170 MeV/c

0.622 (-5)	-0.162 (-5)	0.861 (-5)	-0.313 (-6)	0.181 (-5)
	0.208 (-4)	-0.558 (-5)	0.290 (-5)	0.978 (-5)
		0.601 (-4)	-0.240 (-4)	0.196 (-4)
			0.716 (-4)	-0.334 (-4)
				0.101 (-3)

(H) 2303 MeV/c

0.136 (-5)	-0.173 (-6)	0.132 (-5)	0.333 (-6)	-0.691 (-6)
	0.393 (-5)	-0.957 (-6)	0.138 (-5)	0.409 (-6)
		0.934 (-5)	-0.229 (-5)	0.126 (-5)
			0.131 (-4)	-0.412 (-5)
				0.190 (-4)

TABLE IV. (*Continued*)

(I) 2529 MeV/c

0.134 (-5)	-0.506 (-7)	0.156 (-5)	0.847 (-6)	-0.971 (-7)
	0.396 (-5)	-0.523 (-6)	0.219 (-5)	0.881 (-6)
		0.998 (-5)	-0.143 (-5)	0.267 (-5)
			0.136 (-4)	-0.352 (-5)
				0.190 (-4)

(J) 2595 MeV/c

0.133 (-5)	-0.468 (-6)	0.129 (-5)	0.862 (-6)	-0.264 (-6)
	0.339 (-5)	-0.928 (-6)	0.943 (-6)	0.163 (-5)
		0.829 (-5)	-0.151 (-5)	0.130 (-5)
			0.112 (-4)	-0.349 (-5)
				0.164 (-4)

(K) 2795 MeV/c

0.146 (-5)	0.602 (-7)	0.218 (-5)	0.100 (-5)	0.200 (-6)
	0.476 (-5)	0.873 (-6)	0.198 (-5)	0.240 (-5)
		0.119 (-4)	-0.865 (-6)	0.474 (-5)
			0.139 (-4)	-0.260 (-5)
				0.213 (-4)

(L) 3027 MeV/c

0.107 (-5)	0.342 (-6)	0.174 (-5)	0.529 (-6)	0.510 (-6)
	0.304 (-5)	0.664 (-6)	0.173 (-5)	0.102 (-5)
		0.783 (-5)	-0.123 (-5)	0.360 (-5)
			0.803 (-5)	-0.211 (-5)
				0.116 (-4)

(M) 3101 MeV/c

0.115 (-5)	-0.421 (-6)	0.212 (-5)	-0.271 (-6)	0.730 (-6)
	0.294 (-5)	-0.165 (-5)	0.241 (-5)	-0.187 (-6)
		0.104 (-4)	-0.401 (-5)	0.389 (-5)
			0.961 (-5)	-0.340 (-5)
				0.125 (-4)

(N) 3308 MeV/c

0.936 (-6)	0.380 (-6)	0.176 (-5)	0.812 (-6)	0.728 (-6)
	0.210 (-5)	0.100 (-5)	0.154 (-5)	0.108 (-5)
		0.672 (-5)	0.765 (-6)	0.322 (-5)
			0.606 (-5)	0.162 (-6)
				0.854 (-5)

(O) 3485 MeV/c

0.878 (-6)	0.562 (-6)	0.191 (-5)	0.132 (-5)	0.622 (-6)	0.993 (-6)	-0.250 (-6)
	0.217 (-5)	0.156 (-5)	0.216 (-5)	0.149 (-5)	0.502 (-6)	0.486 (-6)
		0.663 (-5)	0.274 (-5)	0.302 (-5)	0.249 (-5)	-0.268 (-6)
			0.689 (-5)	0.817 (-6)	0.373 (-5)	0.539 (-6)
				0.839 (-5)	-0.803 (-6)	0.383 (-5)
					0.100 (-4)	-0.167 (-5)
						0.118 (-4)

(P) 3687 MeV/c

0.839 (-6)	0.518 (-6)	0.213 (-5)	0.908 (-6)	0.145 (-5)	0.400 (-6)	-0.396 (-7)
	0.180 (-5)	0.163 (-5)	0.176 (-5)	0.183 (-5)	0.256 (-6)	0.589 (-6)
		0.773 (-5)	0.220 (-5)	0.530 (-5)	0.122 (-5)	0.599 (-6)
			0.511 (-5)	0.140 (-5)	0.244 (-5)	0.536 (-6)
				0.937 (-5)	-0.899 (-6)	0.354 (-5)
					0.755 (-5)	-0.121 (-5)
						0.934 (-5)

TABLE IV. (*Continued*)

			(Q) 3762 MeV/c			
0.768 (-6)	0.471 (-6)	0.180 (-5)	0.114 (-5)	0.120 (-5)	0.497 (-6)	0.756 (-7)
	0.131 (-5)	0.127 (-5)	0.157 (-5)	0.153 (-5)	0.209 (-6)	0.592 (-6)
		0.547 (-5)	0.252 (-5)	0.382 (-5)	0.139 (-5)	0.498 (-6)
			0.431 (-5)	0.183 (-5)	0.197 (-5)	0.813 (-6)
				0.630 (-5)	-0.340 (-6)	0.270 (-5)
					0.469 (-5)	-0.865 (-6)
						0.564 (-5)
			(R) 3839 MeV/c			
0.904 (-6)	0.444 (-6)	0.204 (-5)	0.128 (-5)	0.494 (-6)	0.881 (-6)	-0.333 (-6)
	0.211 (-5)	0.138 (-5)	0.202 (-5)	0.150 (-5)	0.103 (-6)	0.862 (-6)
		0.701 (-5)	0.293 (-5)	0.261 (-5)	0.268 (-5)	-0.783 (-6)
			0.646 (-5)	0.139 (-5)	0.298 (-5)	0.122 (-5)
				0.743 (-5)	-0.287 (-6)	0.360 (-5)
					0.905 (-5)	-0.117 (-5)
						0.113 (-4)

ed. These corrections, due to the inefficiency of the system, are of the order of 18–25%. The number of events of the various π^0 final states, along with the number of η^0 events, were then normalized to the overall neutral cross section. The results are presented in Fig. 9. The uncertainties shown have been calculated from a propagation of the statistical uncertainties through the analysis.

V. DISCUSSION OF RESULTS

The total neutral cross section (Fig. 8) drops off rapidly with beam momentum, as does the π^0 charge-exchange cross section which is its dominant contribution to ~2.5 GeV/c (Fig. 9). The $2\pi^0$ and η^0 cross sections also decrease with beam momentum, but more slowly, and the $3\pi^0$, $4\pi^0$, and $5\pi^0$ cross sections remain approximately constant.

Figure 10 shows a comparison of our π^0 cross sections with results from previous experiments and the agreement is in general within the experimental uncertainties, except for the points below 1.6 GeV/c and the points at 2.025 and 2.72 GeV/c.

Figure 6 gives the angular distributions for π^0 charge-exchange production calculated from the Legendre-polynomial series using the amplitudes given in Table I and the error matrices given in Table III. Note the dip at $t \simeq -0.6$ GeV^2 for all momenta, which has been observed previously and is conjectured to be due to the vanishing of the spin-flip amplitude as the ρ trajectory goes to zero. It is possible to compare these angular distributions with those of other experiments[3-9] in a few cases where the data were taken at sufficiently similar incident beam momenta, and in general the agreement is acceptable. For example, in Fig. 11 we

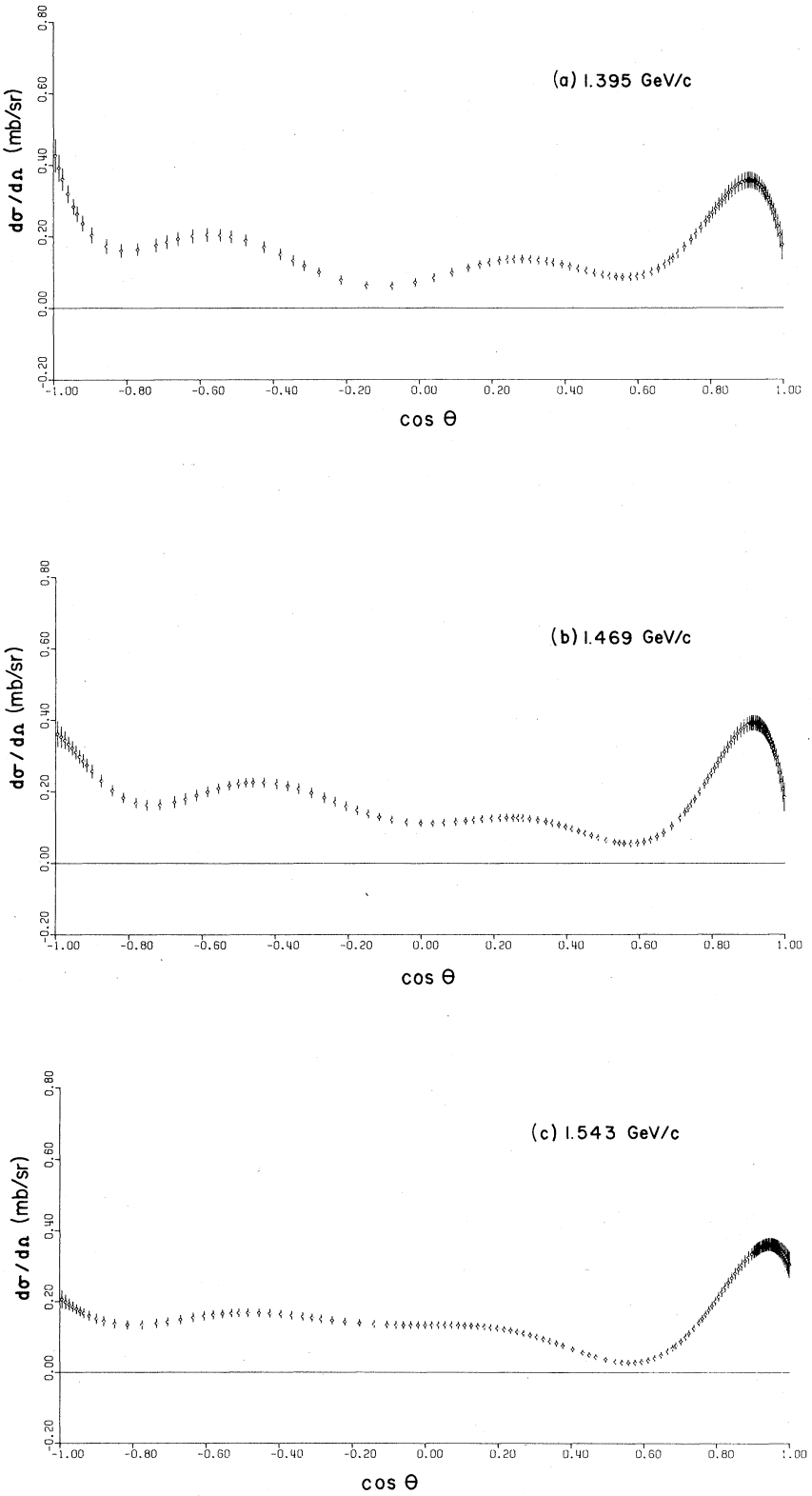

FIG. 6. The center-of-mass differential cross sections as a function of $\cos\theta_{c.m.}$ for $\pi^- + p \rightarrow n + \pi^0$ at 18 values of incident pion laboratory momentum.

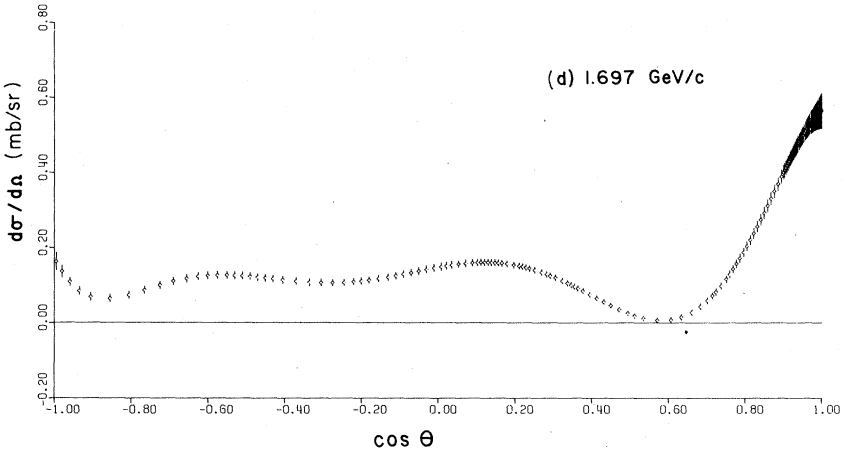

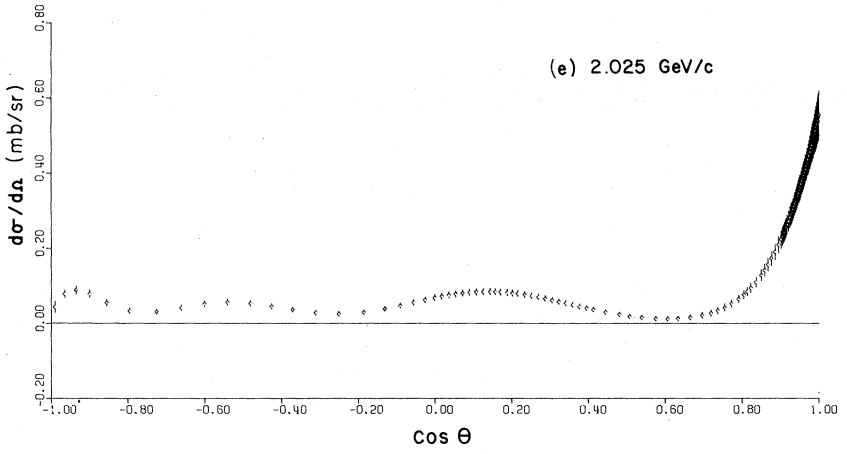

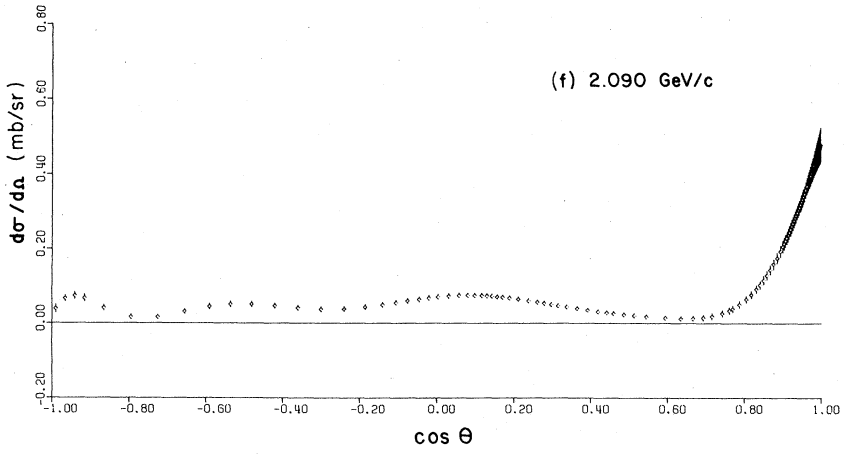

FIG. 6. (*Continued*)

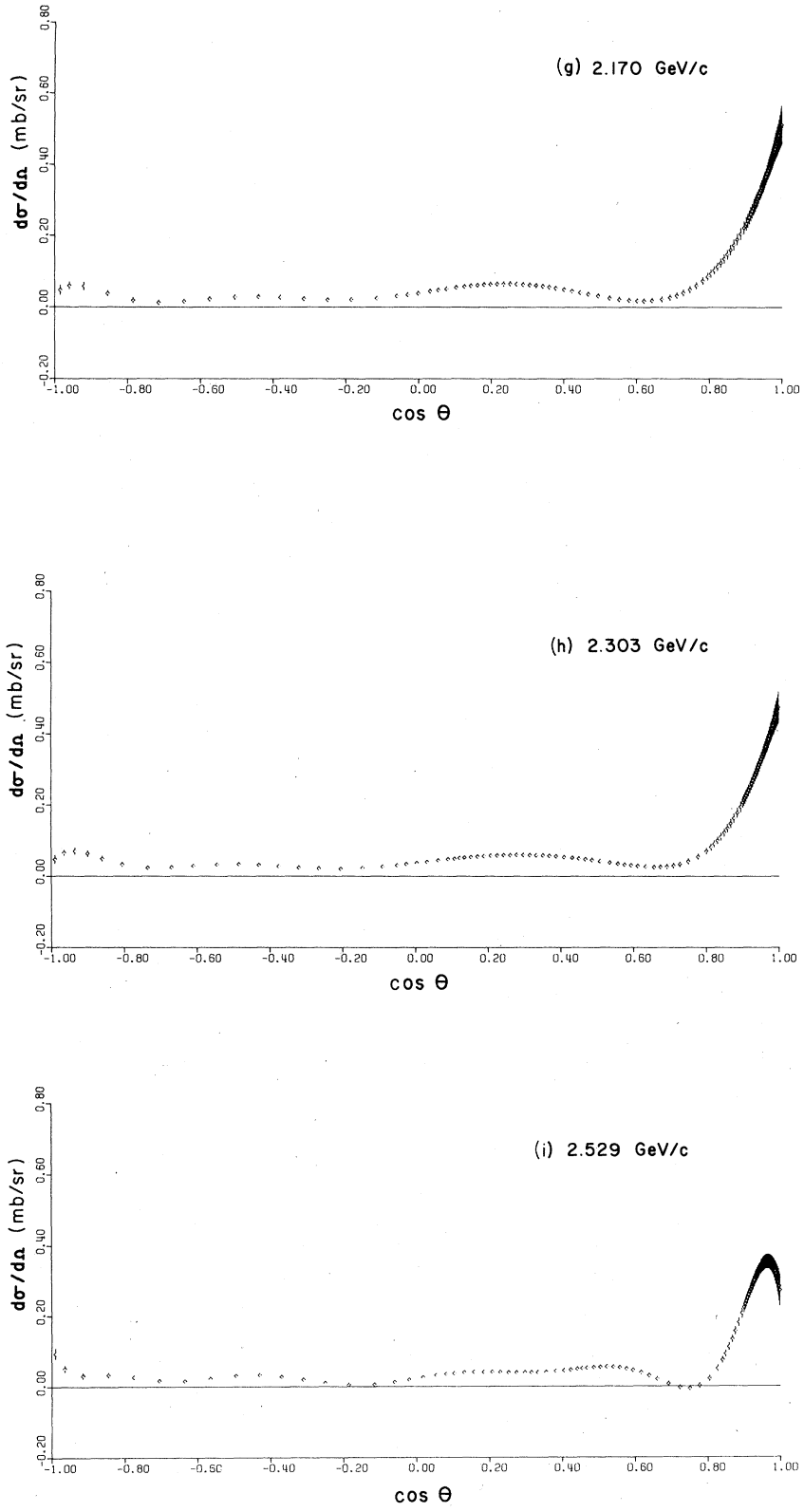

FIG. 6. (*Continued*)

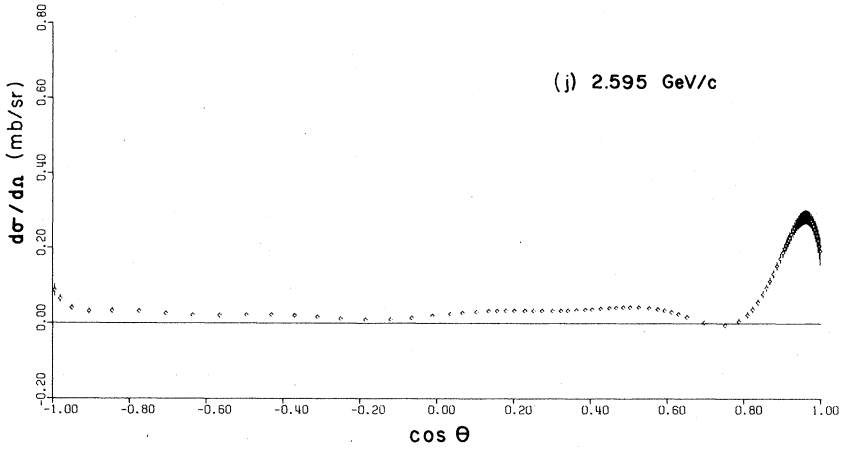

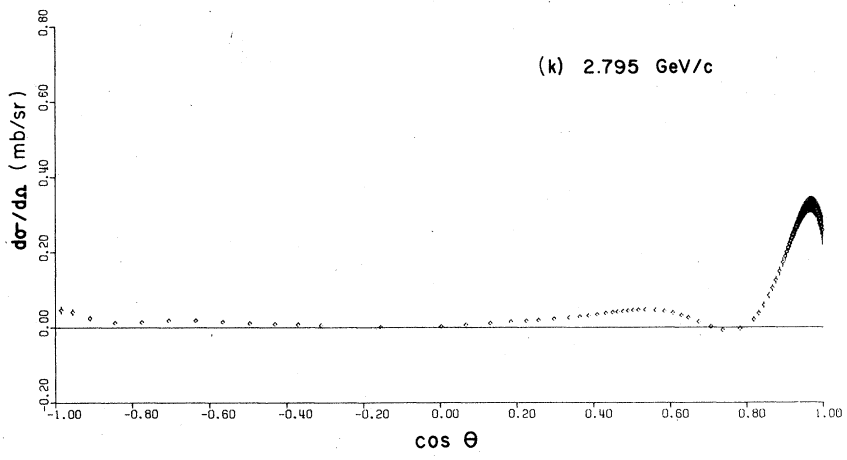

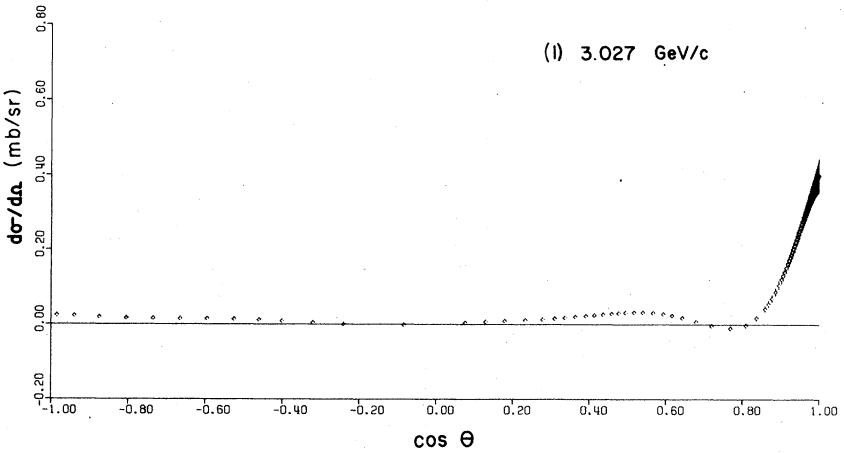

FIG. 6. (*Continued*)

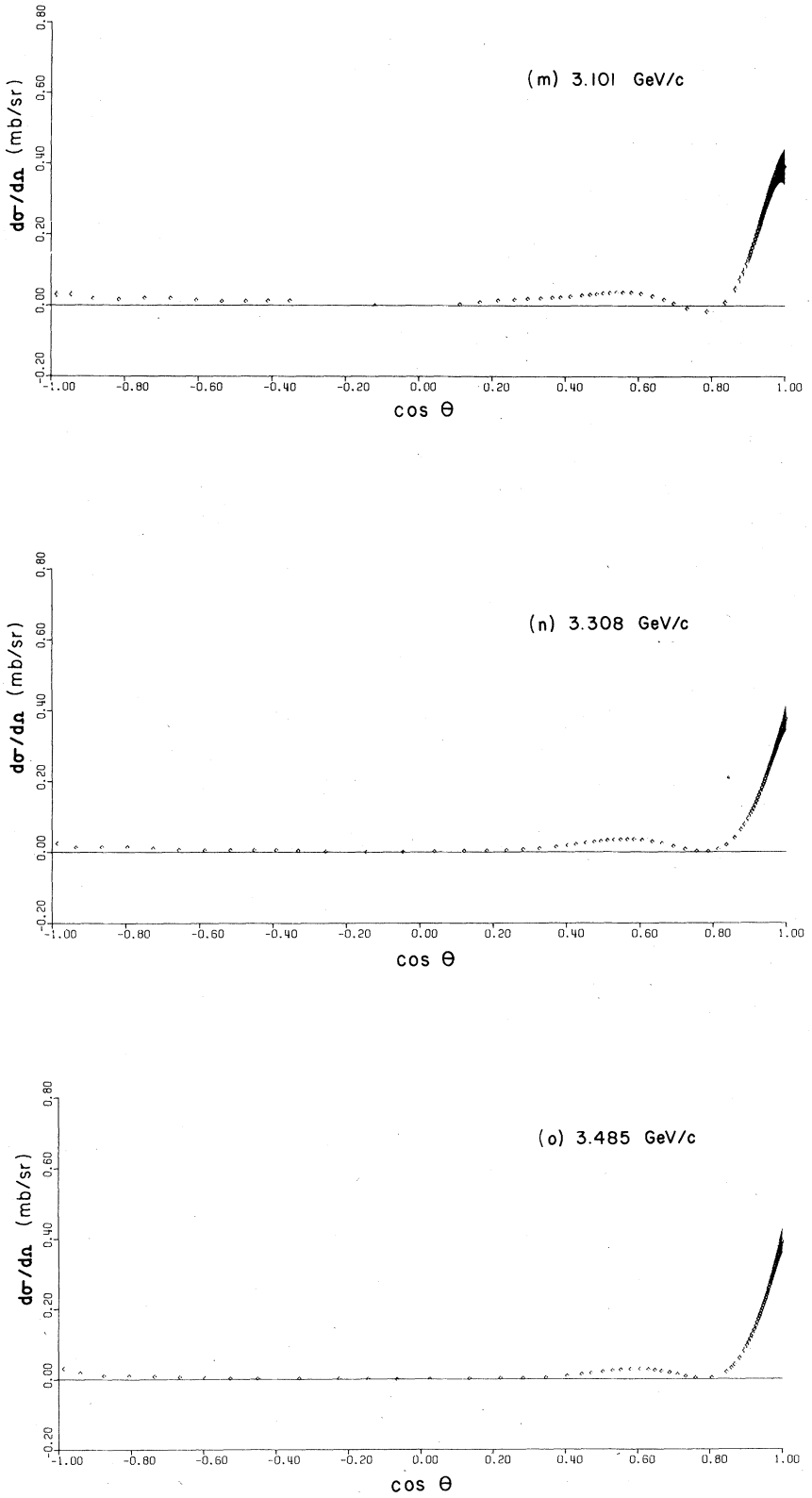

FIG. 6. (*Continued*)

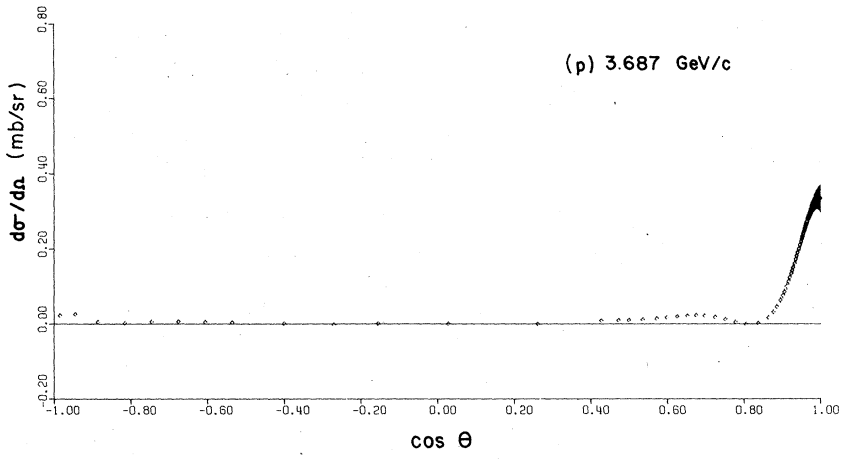

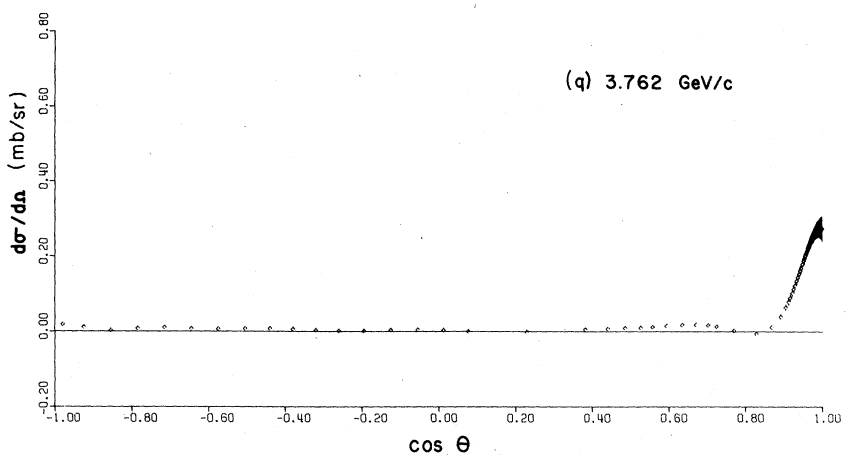

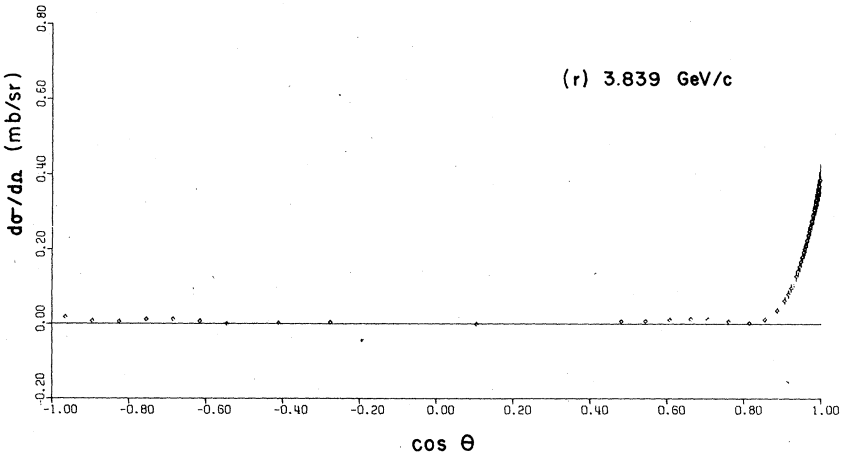

FIG. 6. (*Continued*)

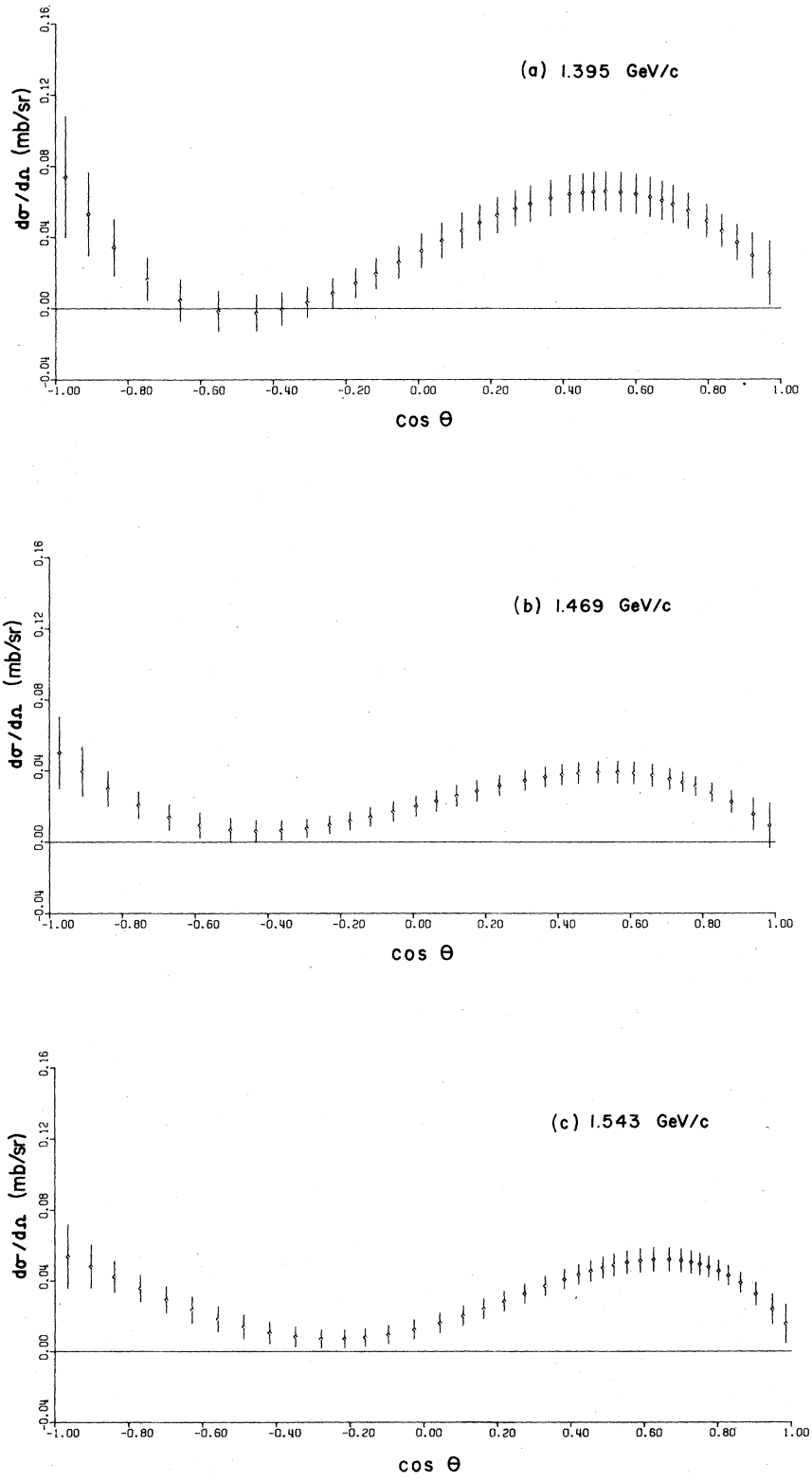

FIG. 7. The center-of-mass differential cross sections as a function of $\cos\theta_{\mathrm{c.m.}}$ for $\pi^- + p \rightarrow n + \eta^0$ at 18 values of incident pion laboratory momentum.

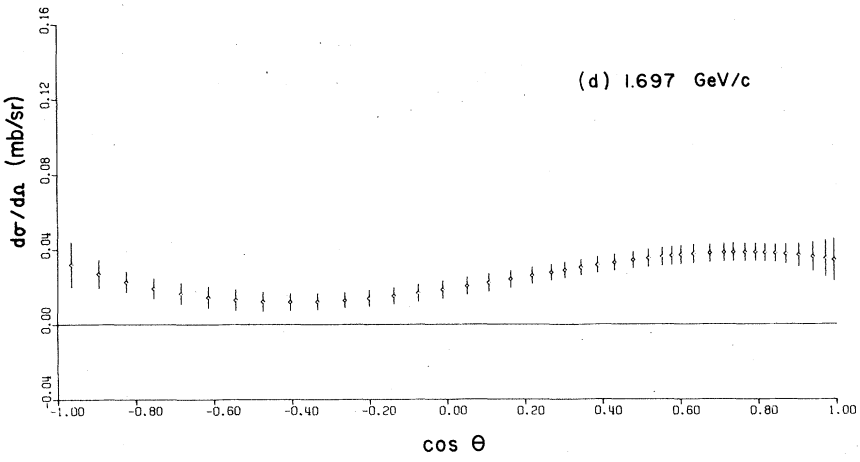

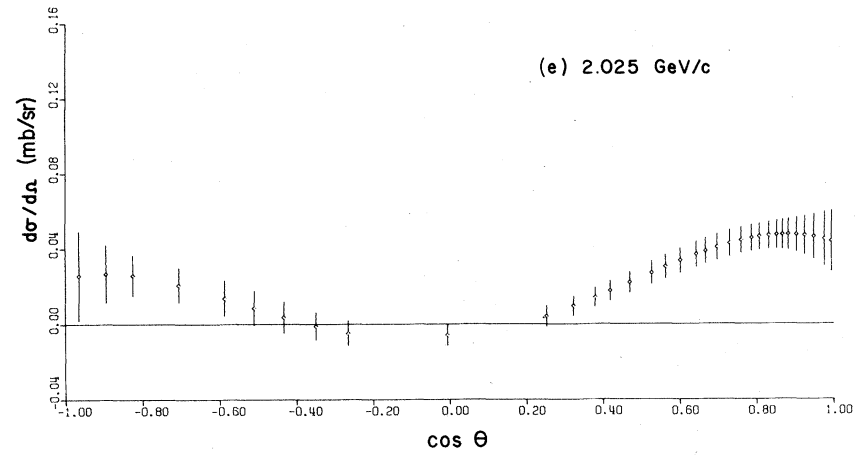

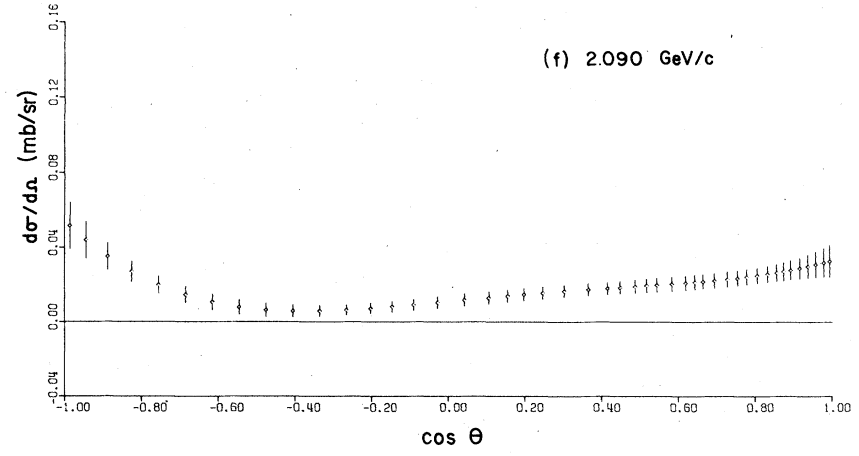

FIG. 7. (*Continued*)

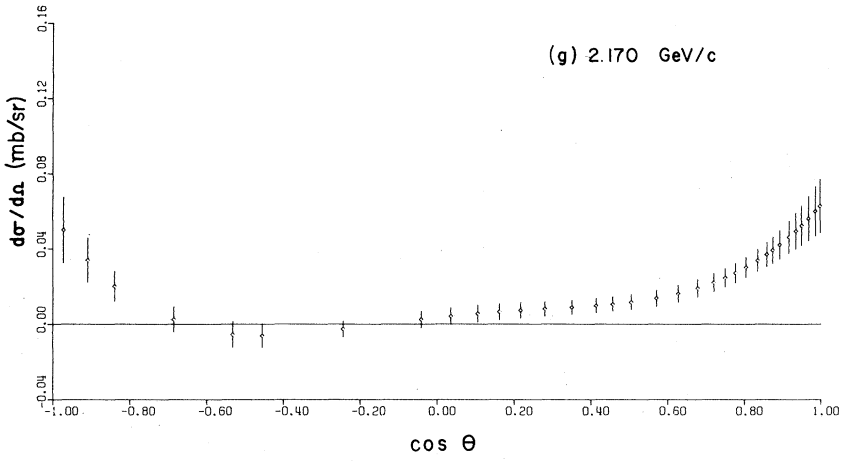

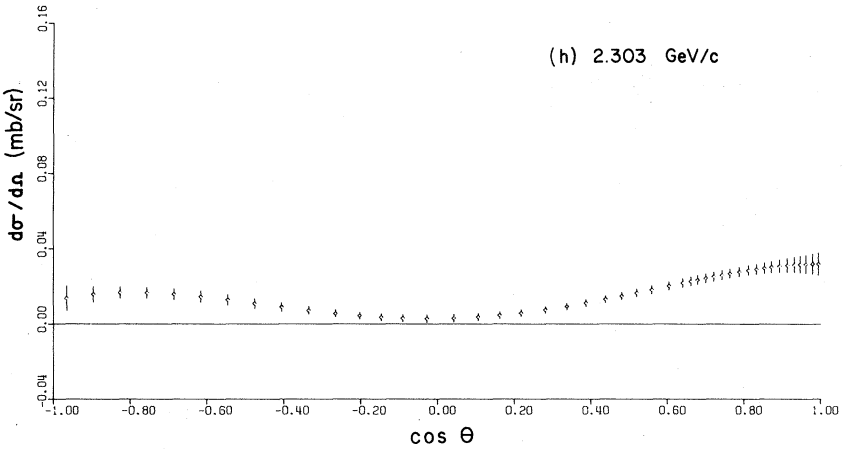

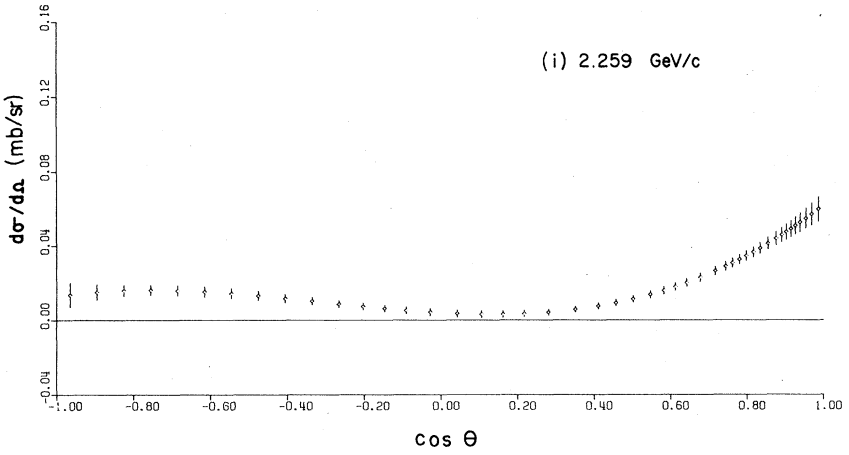

FIG. 7. (*Continued*)

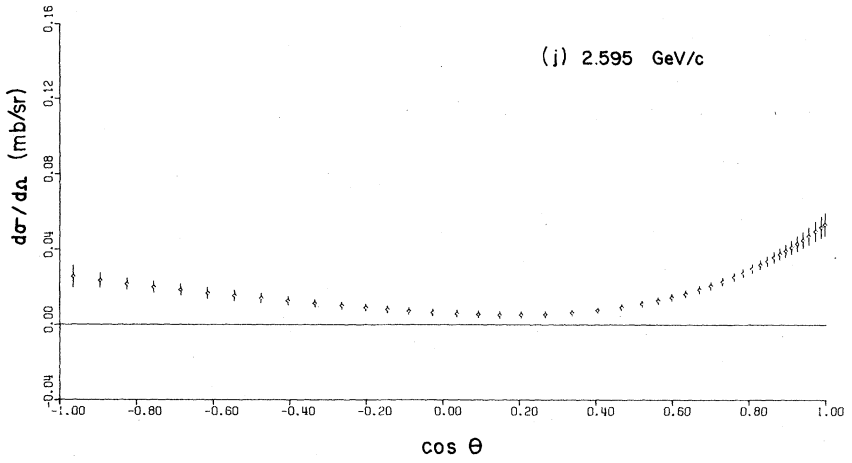

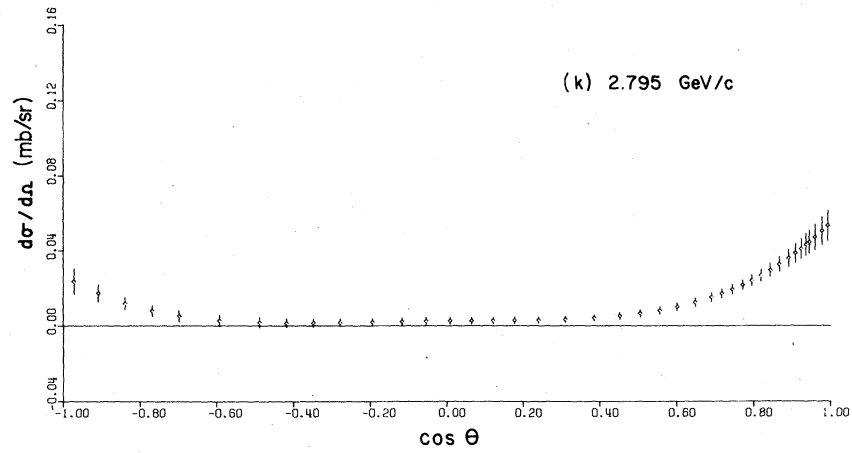

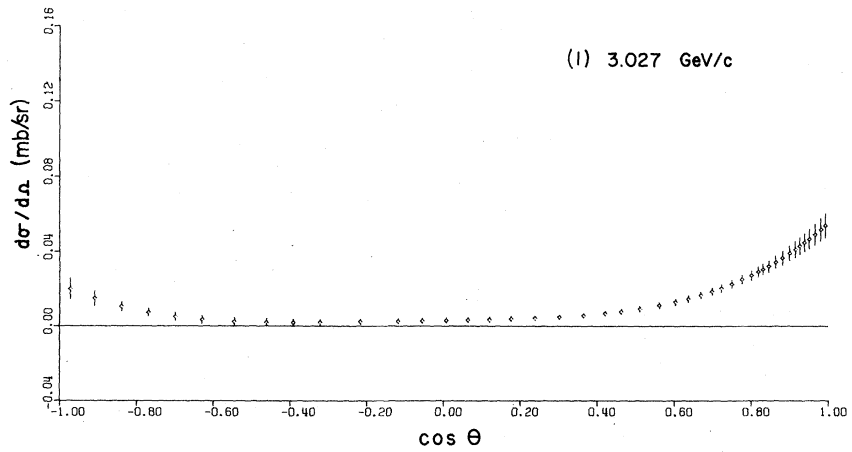

FIG. 7. (*Continued*)

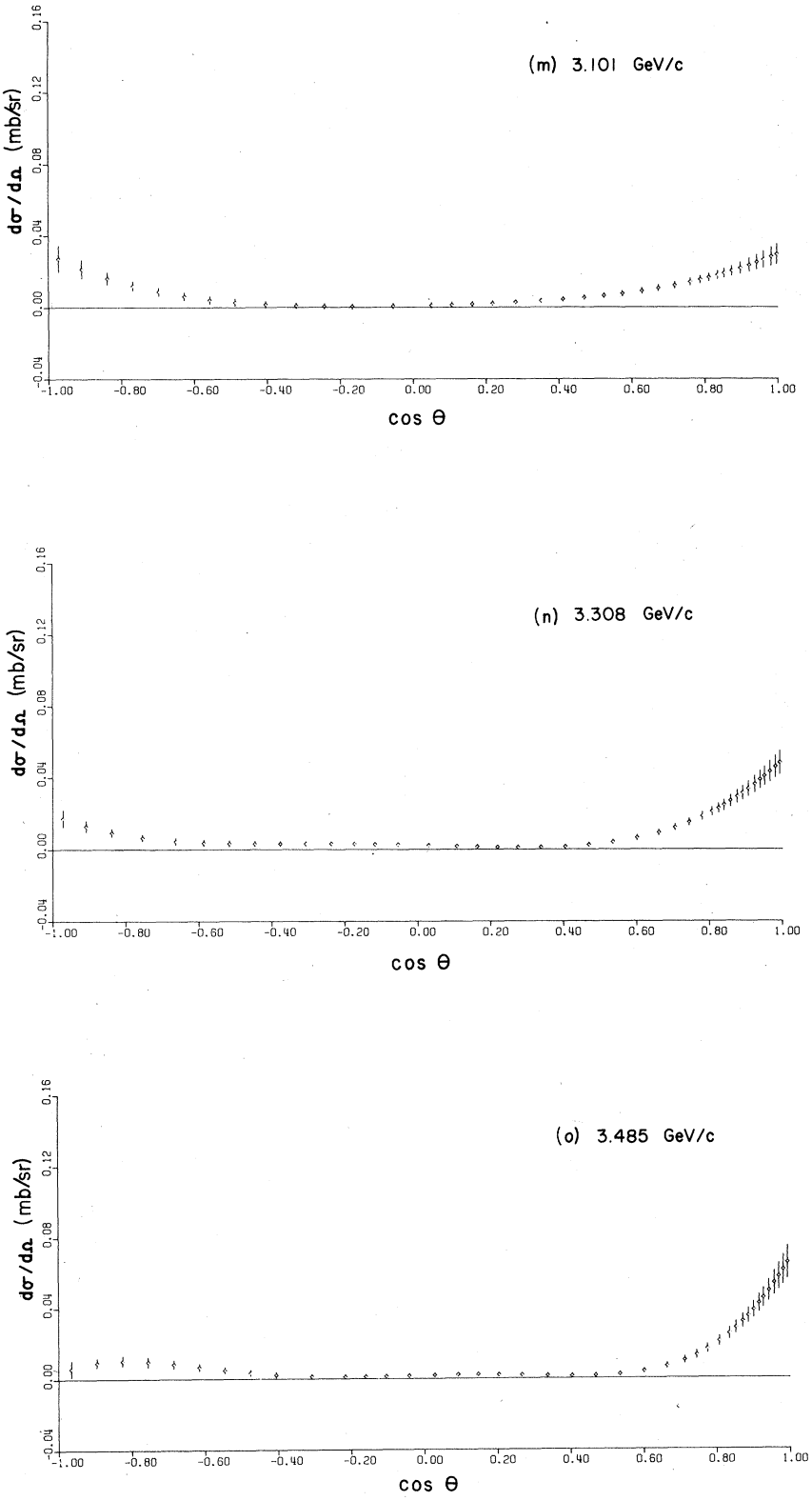

FIG. 7. (*Continued*)

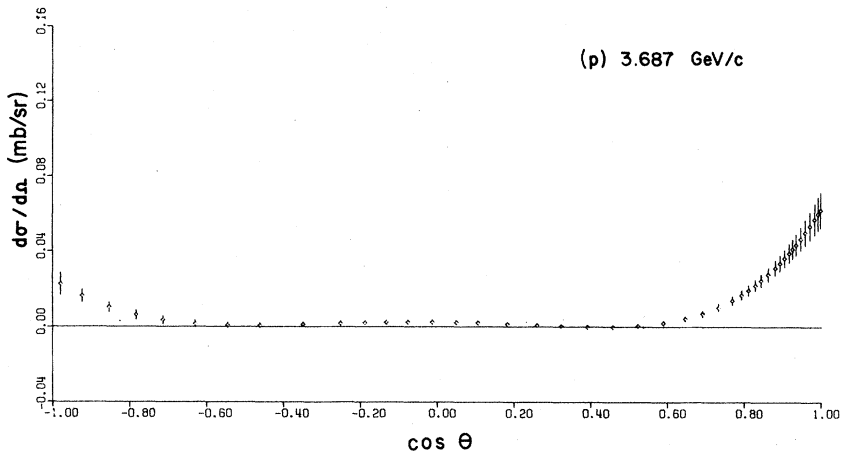

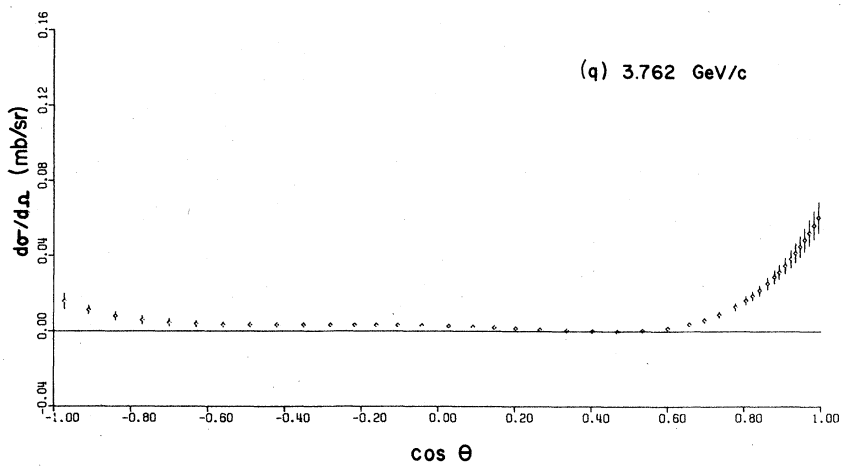

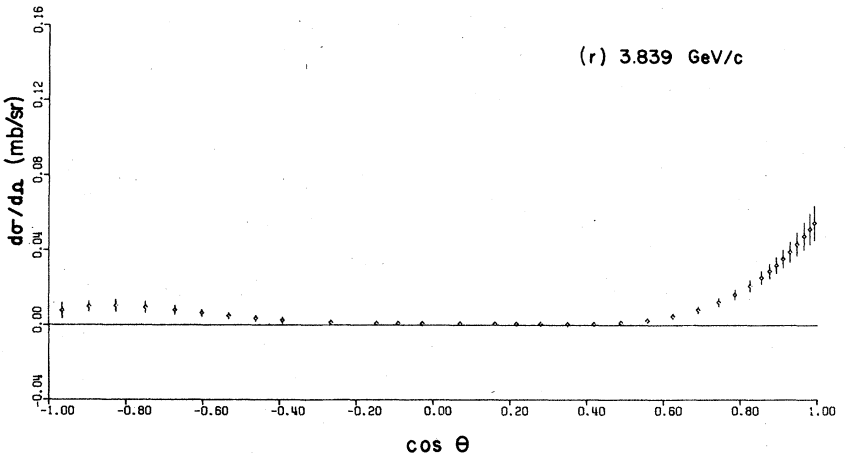

FIG. 7. (*Continued*)

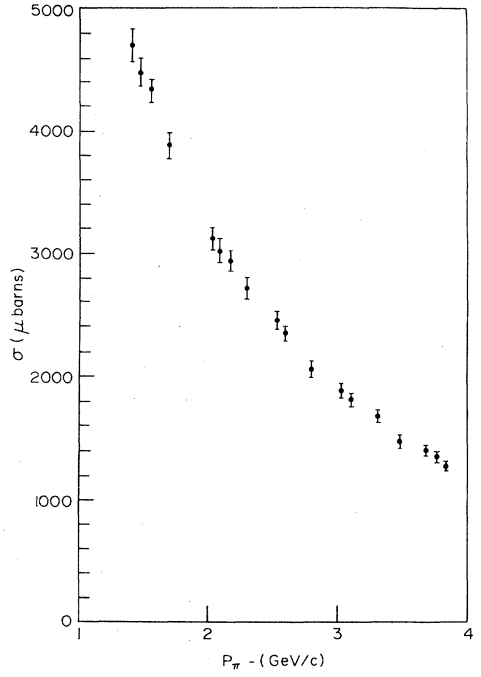

FIG. 8. The total cross section for the prediction of final states with neutral particles only from $\pi^- p$ interactions as a function of incident pion laboratory momentum.

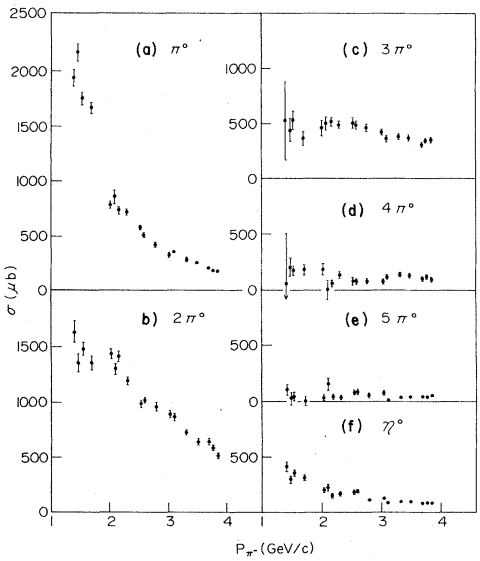

FIG. 9. The total cross sections for the reactions $\pi^- + p \to n + N\pi^0$, where $N = 1$ through 5, and $\pi^- + p \to n + \eta^0$ ($\eta^0 \to 2\gamma$) as a function of incident pion laboratory momentum.

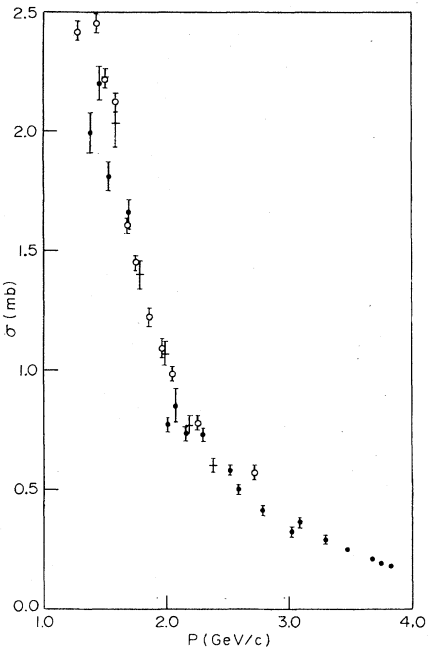

FIG. 10. The total cross sections for $\pi^- + p \to n + \pi^0$ as a function of incident pion laboratory momentum: ●—this experiment, +—Nelson *et al.* (Ref. 5), ○—Brown *et al.* (Ref. 3).

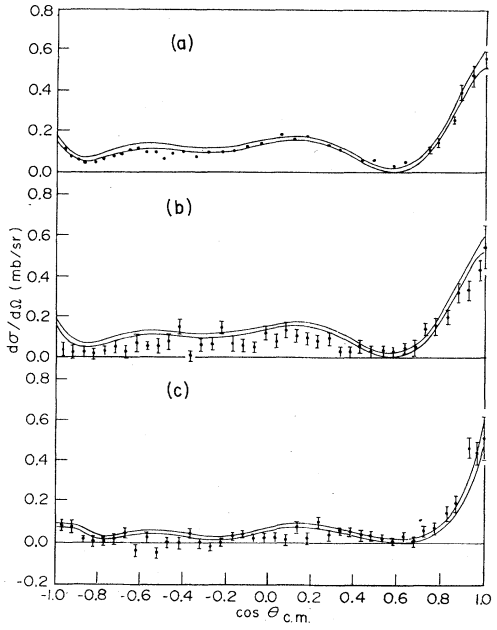

FIG. 11. The center-of-mass differential cross sections for $\pi^- + p \to n + \pi^0$ as a function of $\cos\theta_{\text{c.m.}}$. (a) Solid lines–this experiment at 1697 MeV/c; points–Brown *et al.* (Ref. 3) at 1688 MeV/c. (b) Solid lines–this experiment at 1697 MeV/c; points–Carroll *et al.* (Ref. 4) at 1.71 GeV/c. (c) Solid lines–this experiment at 2090 MeV/c; points–Carroll *et al.* (Ref. 4) at 2.07 GeV/c.

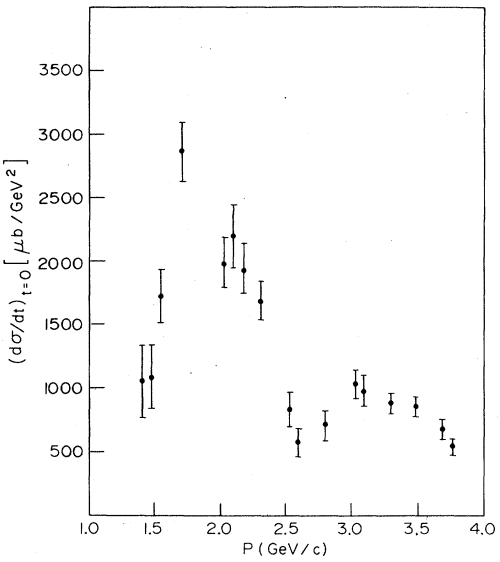

FIG. 12. The differential cross section $d\sigma/dt$ at $t = 0$, for $\pi^- + p \to n + \pi^0$ as a function of incident pion laboratory momentum.

show a comparison of our results with those of Brown *et al.*[3] and Carroll *et al.*[4]

Figure 7 gives the angular distributions for η^0 charge-exchange production calculated from the Legendre-polynomial series using the amplitudes given in Table II and the error matrices given in Table IV. The amplitudes may be compared with

TABLE V. Differential cross section at 0^0 for $\pi^- + p \to n + \pi^0$ at eighteen incident pion momenta.

P (MeV/c)	$\left(\frac{d\sigma}{d\Omega}\right)_{0^0}$ (mb/sr)
1395	0.163 ± 0.045
1469	0.177 ± 0.041
1543	0.302 ± 0.038
1697	0.566 ± 0.048
2025	0.483 ± 0.048
2090	0.557 ± 0.066
2170	0.514 ± 0.055
2303	0.480 ± 0.045
2529	0.267 ± 0.046
2595	0.188 ± 0.039
2795	0.253 ± 0.041
3027	0.402 ± 0.046
3101	0.393 ± 0.052
3308	0.379 ± 0.036
3485	0.393 ± 0.036
3687	0.334 ± 0.039
3762	0.273 ± 0.035
3839	0.390 ± 1.329

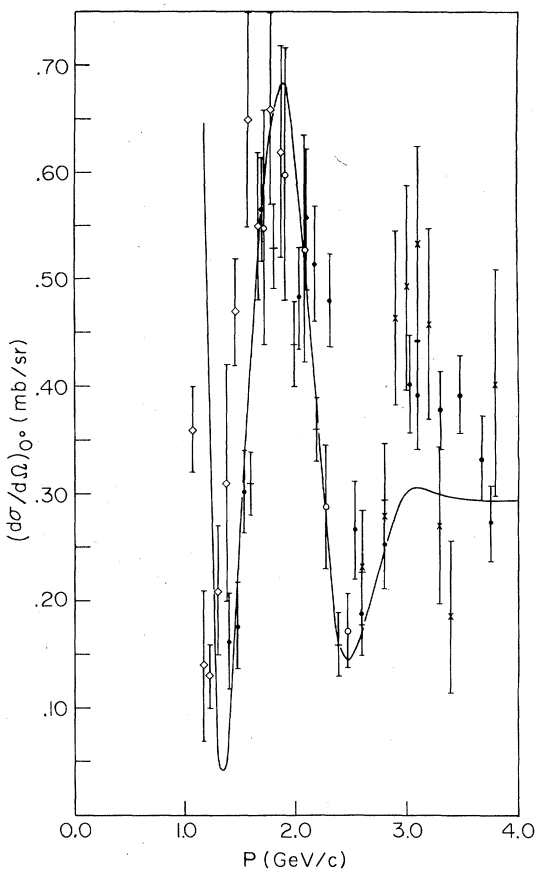

FIG. 13. The differential cross section $d\sigma/d\Omega$ at $\theta = 0^0$, for $\pi^- + p \to n + \pi^0$ as a function of incident pion laboratory momentum. ●—this experiment; ×—Wahlig and Mannelli (Ref. 8); +—Nelson *et al.* (Ref. 5); ◇—Borgeaud *et al.* (Ref. 9); ○—Carroll *et al.* (Ref. 4); solid line—Höhler (Ref. 10).

those obtained for the bisector distribution by Carroll *et al.*[4] at two momenta (1.7 and 2.1 GeV/c) and within the large uncertainties they are in agreement.

The π^0 charge-exchange differential cross sections with respect to four-momentum transfer t at $t = 0$ are shown in Fig. 12, and values for the differential cross sections with respect to Ω at $\theta = 0^0$ are given in Table V. There have been determinations of these differential cross sections by other experiments[3-9] and a comparison is presented in Fig. 13. The solid curve is hand drawn through the points obtained by Höhler *et al.*[11] from phase-shift analysis, and is in reasonable agreement with most of the data below 3 GeV/c. Dispersion relation calculations[12] for the forward cross section have also been carried out and compared with other experimental data, in particular with that of Brown

et al.,[1] but the agreement is not good. Höhler *et al.*[11] suggest that this may occur because the extrapolation to 0^0 depends strongly on the cutoff in the Legendre expansion. We do not present a comparison with the dispersion-relation calculations, because our data are in good agreement with those of previous experiments. For example, Fig. 14 gives a comparison of the values obtained for the Legendre coefficients in this experiment and by Brown *et al.*[3] at similar energies.

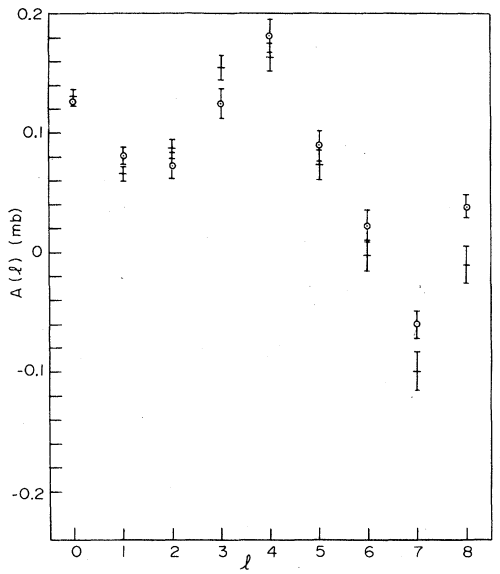

FIG. 14. Legendre-polynomial-series coefficients. $A(l)$ as a function of l obtained by fitting angular distributions from $\pi^- + p \to n + \pi^0$. +—this experiment at 1697 MeV/c; o—Brown *et al.* (Ref. 3) at 1688 MeV/c.

VI. SUMMARY

We have determined the differential cross sections for $\pi^- + p \to n + \pi^0$ and $\pi^- + p \to n + \eta^0$ ($\eta^0 \to 2\gamma$) at 18 energies in the incident π^- momentum interval 1.0–4.0 GeV/c. The charge-exchange differential cross sections at 0^0 are in good agreement with previous work. The dip at $t \simeq -0.6$ GeV^2 is observed at all momenta and there is evidence for a dip at $u \simeq -0.15$ GeV^2. We have also determined total cross sections for π^0 and η^0 charge exchange, the production of two to five π^0's, and for the total neutral cross section.

ACKNOWLEDGMENTS

This work was supported in part by the U. S. Department of Energy and by the Istituto Nazionale di Fisica Nucleare, Rome, Italy. We wish to thank the operating crew of the Brookhaven National Laboratory Alternating Gradient Synchrotron, without whose assistance this experiment could not have been performed, and we wish to thank the scanning and measuring groups at our various universities. In addition, we thank Mr. T. Lyons and Mr. B. Dainese and their groups for expert technical assistance.

*Current address: New College, Sarasota, Florida.
†Current address: Dartmouth College, Hanover, New Hampshire.
‡Current address: University of Arizona, Tucson, Arizona.
§Current address: Fermilab, Batavia, Illinois.
||Current address: Department of Defense, Washington, D. C.
¶Current address: University of California, Los Angeles, California.
**Current address: Bell Labs, Holmdel, New Jersey.
††Current address: Indiana University, Bloomington, Indiana.
‡‡Permanent address: CERN, CH 1211 Genève 23, Switzerland.
§§Current address: Arcon Corporation, Waltham, Massachusetts.
||||Current address: University of Tennessee, Knoxville, Tennessee.
¶¶Current address: CERN, CH 1211 Genève 23, Switzerland.
***Permanent address: University of Padova, Padova, Italy.
†††Current address: Rutgers University, New Brunswick, New Jersey.

[1] H. R. Crouch *et al.*, Phys. Rev. Lett. 21, 845 (1968); 21, 849 (1968).
[2] J. Ashkin *et al.*, Phys. Rev. 101, 1149 (1956); C. B. Chiu *et al.*, *ibid.* 156, 1415 (1967); F. Bulos *et al.*, *ibid.* 187, 1827 (1969); N. C. Debenham *et al.*, Phys. Rev. D 12, 2545 (1975).
[3] R. M. Brown *et al.*, Nucl. Phys. B117, 12 (1976).
[4] A. S. Carroll *et al.*, Phys. Rev. 177, 2047 (1969).
[5] J. E. Nelson *et al.*, Phys. Lett. 47B, 281 (1973).
[6] R. C. Chase *et al.*, Phys. Rev. D 2, 2588 (1970).
[7] P. Sonderegger *et al.*, Phys. Lett. 20, 75 (1966).
[8] M. A. Wahlig and I. Mannelli, Phys. Rev. 168, 1515 (1970).
[9] P. Borgeaud *et al.*, Phys. Lett. 10, 134 (1964).
[10] A. V. Stirling *et al.*, Phys. Rev. Lett. 14, 763 (1965); A. V. Barnes *et al.*, *ibid.* 37, 76 (1976).
[11] G. Höhler *et al.*, Kernforschungzentrum Karlsruhe GmbH Report No. KfK-2735, 1979 (unpublished).
[12] G. Höhler *et al.*, Kernforschungszentrum Karlsruhe GmbH Report No. KfK-2457, 1977 (unpublished).